AGU PUBLICATIONS

Global Biogeochemical Cycles

RESEARCH ARTICLE
10.1002/2015GB005135

Special Section:
Trends and Determinants of the Amazon Rainforests in a Changing World, A Carbon Cycle Perspective

Key Points:
- CO_2 fertilization is a major contributor to the increase in simulated biomass of old growth forests in the last 40 years
- Land use change reduces the simulated Amazon biomass comparable in magnitude to the biomass increase from CO_2 fertilization
- Better representation of mortality from extreme climate events is required in DGVMs

Correspondence to:
A. D. A. Castanho,
adacastanho@gmail.com

Citation:
Castanho, A. D. A., D. Galbraith, K. Zhang, M. T. Coe, M. H. Costa, and P. Moorcroft (2016), Changing Amazon biomass and the role of atmospheric CO_2 concentration, climate, and land use, *Global Biogeochem. Cycles*, *30*, 18–39, doi:10.1002/2015GB005135.

Received 6 MAR 2015
Accepted 29 OCT 2015
Accepted article online 6 NOV 2015
Published online 19 JAN 2016

Changing Amazon biomass and the role of atmospheric CO_2 concentration, climate, and land use

Andrea D. de Almeida Castanho[1,2], David Galbraith[3], Ke Zhang[4,5], Michael T. Coe[2], Marcos H. Costa[6], and Paul Moorcroft[5]

[1]Department of Agricultural Engineering, Universidade Federal do Ceará, Ceará, Brazil, [2]Woods Hole Research Center, Falmouth, Massachusetts, USA, [3]School of Geography, University of Leeds, Leeds, UK, [4]Cooperative Institute for Mesoscale Meteorological Studies, University of Oklahoma, Norman, Oklahoma, USA, [5]Department of Organismic and Evolutionary Biology, Harvard University, Cambridge, Massachusetts, USA, [6]Department of Agricultural Engineering, Universidade Federal de Viçosa, Viçosa, Brazil

Abstract The Amazon tropical evergreen forest is an important component of the global carbon budget. Its forest floristic composition, structure, and function are sensitive to changes in climate, atmospheric composition, and land use. In this study biomass and productivity simulated by three dynamic global vegetation models (Integrated Biosphere Simulator, Ecosystem Demography Biosphere Model, and Joint UK Land Environment Simulator) for the period 1970–2008 are compared with observations from forest plots (Rede Amazónica de Inventarios Forestales). The spatial variability in biomass and productivity simulated by the DGVMs is low in comparison to the field observations in part because of poor representation of the heterogeneity of vegetation traits within the models. We find that over the last four decades the CO_2 fertilization effect dominates a long-term increase in simulated biomass in undisturbed Amazonian forests, while land use change in the south and southeastern Amazonia dominates a reduction in Amazon aboveground biomass, of similar magnitude to the CO_2 biomass gain. Climate extremes exert a strong effect on the observed biomass on short time scales, but the models are incapable of reproducing the observed impacts of extreme drought on forest biomass. We find that future improvements in the accuracy of DGVM predictions will require improved representation of four key elements: (1) spatially variable plant traits, (2) soil and nutrients mediated processes, (3) extreme event mortality, and (4) sensitivity to climatic variability. Finally, continued long-term observations and ecosystem-scale experiments (e.g. Free-Air CO_2 Enrichment experiments) are essential for a better understanding of the changing dynamics of tropical forests.

1. Introduction

Increasing atmospheric CO_2, changing climate and land cover/land use change are three important factors acting on the world's forests, potentially altering their carbon balance in both positive and negative ways. Increasing CO_2 is expected to boost plant photosynthetic rates directly and also to improve water use efficiency resulting in an enhancement of terrestrial carbon sinks assuming there are no changes in the allocation of photosynthates and turnover time of carbon [*Lloyd and Farquhar*, 1996]. Changing climate can further enhance or diminish terrestrial C sinks, depending on water availability and temperature constraints [*Reichstein et al.*, 2013; *Zscheischler et al.*, 2014]. Furthermore, at larger spatial scales land use change exerts a strong control on the regional C balance as large swathes of the world's major biomes have been converted for agricultural use [*Foley et al.*, 2011].

Spanning an area of ~$7 \times 10^6 km^2$, the Amazon forest is thought to be a significant atmospheric carbon sink [*Phillips et al.*, 2008]. Given their size, any widespread changes in the C balance of Amazonian forests could directly affect global climate and have important implications for mitigation policies designed to stabilize greenhouse gases levels [*Aragão et al.*, 2014; *Houghton*, 2014; *Pan et al.*, 2011]. Thus, accurate understanding and representations of the response of tropical forests to changing environmental resources (atmospheric CO_2 concentrations, temperature, water availabilitys, nutrients, and light) and land use change are essential for robust future predictions of the global carbon cycle.

Long-term forest inventory studies of old-growth forests across Amazonia have documented an increase in aboveground biomass in recent decades [*Baker et al.*, 2004; *Lewis et al.*, 2004c; *Phillips et al.*, 2008;

Phillips et al., 1998]. The authors of these studies have pointed to increasing atmospheric CO_2 as the most likely driver of the observed Amazonian forest carbon sink. Other possible drivers that have been highlighted include climate variations, increasing nutrient mineralization rates, and increases in diffuse radiation due to increasing atmospheric aerosol loads resulting from biomass burning; each of these possibilities are discussed in detail in [*Lewis et al.*, 2004b, 2009]. Another hypothesis suggests that the increase in biomass could be a recovery from large-scale past disturbances, such as drought [*Clark et al.*, 2010; *Muller-Landau*, 2009; *Wright*, 2013]. Although this may be true for specific monitoring sites across the study area (as for example in Tapajos in Brazilian Amazonia), [*Lewis et al.*, 2004c], the very long return times of such disturbance events across the study area makes their large-scale impact less clear [*Espirito-Santo et al.*, 2014].

In this study dynamic global vegetation models (DGVMs) are used to explore the contributions of CO_2, climate, and land use to changes in the Amazonian C balance between 1970 and 2008. While DGVMs have frequently been used in assessments of the impacts of future climate change on Amazonian forests [*Galbraith et al.*, 2010; *Huntingford et al.*, 2013; *Rammig et al.*, 2010; *Zhang et al.*, 2015], there has been little evaluation of their ability to simulate biomass dynamics as observed by field measurements. Forest plot data on biomass dynamics reflect the contributions of several external forces, including short and long-term climate variability and disturbances (e.g., fire and blowdown events) as well as long-term increases in atmospheric CO_2 concentration. DGVMs can help to separate the individual effects of climate, increasing atmospheric CO_2 concentrations, land use change or fire, on carbon stocks, and fluxes. In undisturbed forests, where long-term measurement plots are located, DGVMs provide a test for the hypothesis that CO_2 fertilization is the major mechanism driving the observed increase in biomass of undisturbed forest plots. In this study, a suite of simulations is conducted using three DGVMs to isolate the individual and combined effects of CO_2, climate, and land use change on the long-term Amazonian C balance (1970–2008). The ability of the DGVMs to reproduce biomass responses to long-term (e.g., decadal climatic variation) and short-term (e.g., single-year drought events) forcings is evaluated.

2. Material and Methods

2.1. Dynamic Global Vegetation Models Description

We use three Dynamic Global Vegetation Models (DGVM): the Integrated Biosphere Simulator (IBIS) [*Foley et al.*, 1996; *Kucharik et al.*, 2000], the Ecosystem Demography Biosphere Model (ED2) [*Medvigy et al.*, 2009; *Moorcroft et al.*, 2001], and the Joint UK Land Environment Simulator Model (JULES, v2.1) [*Best et al.*, 2011; *Clark et al.*, 2011]. IBIS, and JULES simulate community dynamics and competition between plant functional types (PFTs) using an aggregated "big-leaf" representation of the plant canopy within each climatological grid cell. ED2 represents tree population, size and age structure explicitly, simulating individual plant-scale dynamics and competition. A summary of the exclusive processes and parameterizations that the models use is described below and is summarized in Table 1; detailed additional information on the C3 plant physiological processes are described in Tables A1 and A2 in Appendix A. The basic functions are the same between the models; however, parameterization and specific factors that modulate photosynthesis and stomatal conductance, such as water stress factors and phenology differ between the models, causing differences in simulated vegetation sensitivity to CO_2 fertilization and water stress. A detailed description of the models can be found in the original model description papers.

2.2. Numerical Models Simulations Protocol

The application of all DGVMs followed a common protocol, being forced with the same climate and soil conditions [*Zhang et al.*, 2015]. The region of study was delimited by the Amazon watershed and the Guiana Shield region to the north, with a total area of 8×10^6 km^2 (Figure 1). The simulations were made at $1 \times 1°$ horizontal spatial resolution with an hourly time step for the 39 year period from 1970 to 2008. During this period the models were forced with prescribed hourly climate based on the *Sheffield et al.* [2006] database, which is a combination of global observation-based data sets and reanalysis data from the National Center for Environmental Prediction-National Center for Atmospheric Research. The year 1970 was chosen as a start date of our analysis because it is the point at which the weather station network over Amazonia was sufficiently dense to provide reliable climate records [*Costa et al.*, 2009]. Atmospheric CO_2 concentrations were generated by fitting an exponential function to the ice core data (1700–1959) concatenated with the observed CO_2 concentrations for the historical period (1959–2008) [*Zhang et al.*, 2015]. All DGVMs followed

Table 1. Summary of Relevant Properties and Processes of the DGVMs Used in This Study

	IBIS	ED2	JULES
		Processes	
Representation of plant canopy	Big-leaf	Size and age-structured individual scale	Big-leaf
Plant functional types	Tropical broadleaf evergreen trees; Tropical broadleaf deciduous trees; shrubs; C3, C4 grasses	Tropical plant functional type: fast-growing pioneer tropical trees; midsuccessional tropical trees; slow-growing, shade-tolerant late successional trees; C3 grasses and forbs; and C4 grasses and forbs	Broadleaf evergreen trees; shrubs; C3 and C4 grasses
Nitrogen and phosphorous cycle	Nitrogen cycle not in use Phosphorous cycle none	Nitrogen cycle not in use Phosphorous cycle none	None
Plant carbon pools	Leaf; wood; fine root	Leaf; sapwood; heartwood; fine root; storage; seeds	Leaf; stem; (fine) root
Fractional NPP allocation	30% Leaf; 50% wood; 20% root	Dynamical allocation constrained by PFT-specific allometric equations	Allocation following allometric relationships
Canopy photosynthesis and stomatal conductance (Tables A1 and A2)	*Ball et al.* [1986], *Collatz et al.* [1992], *Collatz et al.* [1991], *Farquhar et al.* [1980], and *Leuning* [1995]	*Ball et al.* [1986], *Collatz et al.* [1992], *Collatz et al.* [1991], *Farquhar et al.* [1980], and *Leuning* [1995]	*Collatz et al.* [1992], *Collatz et al.* [1991], and *Jacobs* [1994]
Nutrient limitation of CO_2 fertilization	No	No	No
Mortality	Biomass turnover rates of carbon pools function of PFT	Density independent (tree-fall and aging) and density dependent (carbon starvation)	Biomass turnover rates of carbon pools function of PFT
Drought Mortality	No	Drought mortality is an empirical function of carbon balance	No
Mortality due to disturbances	Fixed background disturbance rate	Fixed background disturbance rate	Fixed background disturbance rate
Fire	Function of total litter and available water content	Function of aboveground biomass and available water	No
Forest succession	No	Yes	No
Physiological acclimation to temperature	No	No	No
Soil water distribution	Green-Ampt infiltration parameterization [*Green and Ampt*, 1911]	The dynamics of soil water, is governed by a simple one-layer hydrology model and a modification of the Century model [*Moorcroft et al.*, 2001]	The vertical fluxes follow Darcy's law [*Best et al.*, 2011]
Root water uptake	Asymptotic root distribution function [*Li et al.*, 2005]	The dynamics of soil water is governed by a simple one-layer hydrology model and a modification of the Century model [*Moorcroft et al.*, 2001]	Root density, assumed to follow an exponential distribution with depth. [*Coe et al.*, 2013]
		Parameterization	
Spatial variation of plant traits	IBIS_HP version yes Regular IBIS no	No	No
Temporal variation of plant traits	No	No	No

a spin-up protocol starting from bare ground until soil carbon, vegetation structure, and biomass achieved an equilibrium state. Detailed maps of land use change in the Brazilian Amazon are only available since 1988, via the PRODES product. The historical land use transition rates used in the study were calculated from the Global Land-Use data set (GLU), from 1700 up to 2009 [*Hurtt et al.*, 2006]. The model simulations start from near bare ground and the models were run for a 400 year period with preindustrial CO_2 and recycling the 39 year meteorological forcing data (1970–2008) to bring the carbon pools to equilibrium state at 1700. From 1700 onward, land use and CO_2 concentrations were applied following observational data sets, described above, and the meteorological data set was recycled as per the spin-up period. From 1970 to 2008, we conducted factorial simulations to isolate the effects of climate, land use, and CO_2 concentrations, as described in Table 2a. Land use change (deforestation) was represented in all models by replacing native vegetation with grass. All models used standardized maps of soil texture, the same pedotransfer functions for determining soil physics, and a soil depth of 10 m throughout the study area. In all models the plant rooting depth extends to the full depth of the soil column.

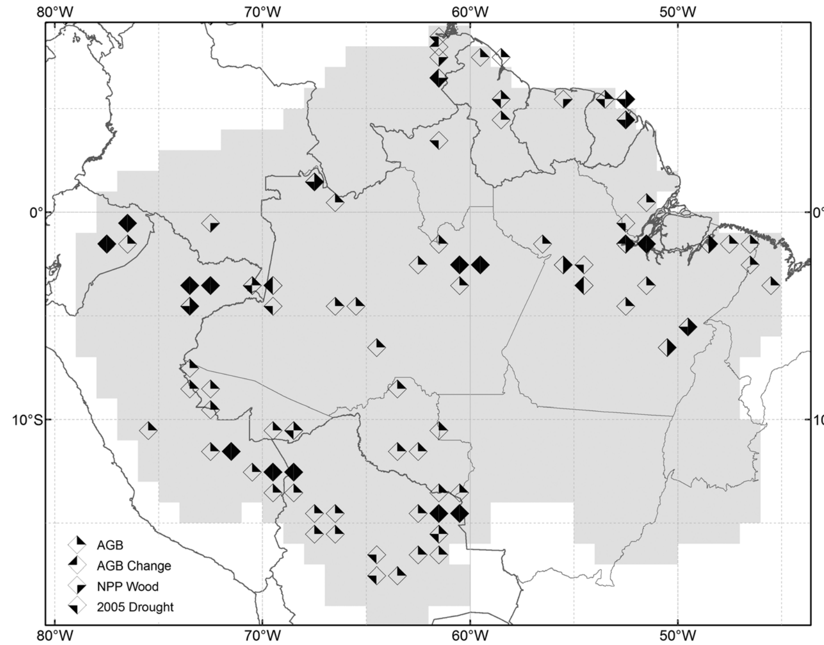

Figure 1. Map showing the Amazon forest study area in gray and the forest monitoring site locations for each property. The shaded area includes the Amazon River study area and tropical forest areas in the north (Guiana) [*Eva et al.*, 2005]. Each triangle in the diamond symbol represents one property. Starting with the aboveground biomass in the top right [*Malhi et al.*, 2006]; woody net primary productivity, in the botton right [*Malhi et al.*, 2004]; change in aboveground biomass, top left [*Baker et al.*, 2004; *Lewis et al.*, 2004c]; analyzed 2005 drought and pre drought, bottom left [*Phillips et al.*, 2009].

A suite of simulations was performed in order to reproduce the individual and combined effects of climate, CO_2 fertilization, land use, and fire changes on the vegetation (Table 2b). The factorial design of the simulations took into account the following: constant atmospheric CO_2 concentration from 1970 (325.7 ppm) and increasing historical atmospheric CO_2 concentration since 1970, simulations with potential vegetation, with land use change, and with and without fire. We use 1970 as the reference year for switching CO_2 on/off for consistency with the available climate data and because our oldest field observations start in the 1970s, more specifically in 1971 [*Lewis et al.*, 2004c]. With this set of simulations it was possible to derive the effect of all factors combined on the vegetation properties (all combined, HistD: current climate, increasing CO_2, land use change, and fire). The individual effect of CO_2 fertilization was taken as the difference between two simulations, one applying constant CO_2 at 1970 values through the period of analyses (HistE) and another allowing for increasing CO_2 concentrations during our study period (HistB). The individual effect of land use change was also taken as the difference between two simulations, one with constant land cover (HistA) and another with historical changes in land cover included (HistD). HistE simulates the effect of climate variability on the

Table 2a. Description of Factorial Simulations Performed From 1970 up to 2008[a]

Simulation	Historical Climate Sheffield 1970–2008	Atmospheric CO_2	Vegetation	Natural Disturb Fire[b]
Hist A	Historical	Increasing	Potential Vegetation	Fire
Hist B	Historical	Increasing	Potential Vegetation	No
Hist C	Historical	Constant (1970, 325.7 ppm)	Potential Vegetation	Fire
Hist D	Historical	Increasing	Land Use	Fire
Hist E	Historical	Constant (1970, 325.7 ppm)	Potential Vegetation	No
IBIS_HP[c]	Historical	Increasing	Potential Vegetation	No

[a]All the simulations (HistA to Hist E) starts from the same initial state resulting from a spin up to preindustrial equilibrium up to 1700 and runs forward until 1970 by accounting for historical gradually rising atmospheric CO_2 (1700–1970), land use change, natural disturbance (fire), and the recycling 1970–2008 climatology.
[b]Fire was simulated in all models except for JULES.
[c]Simulation with modified version of IBIS that includes heterogeneous parameterization across Amazon Basin [*Castanho et al.*, 2013].

Table 2b. Description of the Individual and Combined Effect Studied

Combined Simulations	Analyses
Hist A	Climate and CO_2 Fertilization
Hist B-Hist E	CO_2 Fertilization
Hist D-Hist A	Land Use
Hist D	All Combined
Hist E	Climate
IBIS_HP	Heterogeneous Parameterization

vegetation. Because CO_2 concentrations in HistE were frozen at the 1970 level, this climate analysis includes not only the effect of climate but also any lag effect on the biomass of the increasing CO_2 prior to 1970. Although this is different from the standard in the literature (freezing at preindustrial level, or 280 ppm), we believe this experiment setup is best suited to the problem analyzed here. If we used 280 ppmv as the baseline, we would simulate the response of the vegetation to climate under a nonrepresentative CO_2 concentration for the period covered by the data (1970–2008).

In order to clarify the role of spatial variation in plant traits a sixth simulation with potential vegetation and increasing CO_2 concentration was included using a newer version of IBIS (called IBIS_HP), which included spatially varying plant traits parameterization [*Castanho et al*., 2013]. The spatial varying parameterizations include residence time of carbon in woody biomass, maximum carboxylation capacity of Rubisco (V_{max}), and specific leaf area index. All parameters were derived from RAINFOR network data and were extrapolated to the entire basin. A detailed description of the methods used is in *Castanho et al*. [2013].

Natural fire estimates were included in the simulations but the results are not explored in this work because the contribution to biomass change was very small compared to any other factor.

The analysis focused mainly on the spatial and temporal patterns of aboveground biomass (AGB) and woody net primary productivity (NPP_w) (Table 3). These were explored in two ways: (a) evaluation of model simulated average and spatial gradients of AGB and NPP_w across the Amazon study area and (b) examination of the simulated temporal dynamics of biomass and productivity, here referred to as AGB change (ΔAGB; or fractional change fΔAGB) and growth rate change (fΔNPP_w). In all plot-level data-model comparisons, an evaluation time period of the models was selected that was identical to the census interval periods from the field data.

Climatic water stress was quantified using two measures: dry season length (DSL), which is the duration of the dry season, and maximum cumulative water deficit (MCWD), which is the intensity of the water stress [*Malhi et al*., 2009]. DSL is defined based on the number of months with less than 100 mm month^{-1} rainfall in a given year. The calculation of MCWD involves calculating a water deficit for a given grid cell for a particular month based on the assumption that evapotranspiration is 100 mm month^{-1}. These deficits are then accumulated over all consecutive months in which precipitation is less than 100 mm to calculate MCWD [*Malhi et al*., 2009].

2.3. Field Data for Model Comparison

We assembled a wide range of published data from field observations at several sites across the Amazon study area for evaluation of model results (Figure 1 and Table 3). The sites are all in undisturbed old-growth forest, with most of them being part of the RAINFOR network (*Rede Amazónica de Inventarios Forestales*, Amazon Forest Inventory Network; www.rainfor.org). The RAINFOR project is an international effort to monitor structure, composition, and dynamics of the Amazonian forest in order to better understand their relationship to soil and climate [*Malhi et al*., 2002; *Peacock et al*., 2007]. The RAINFOR field data are plot-level

Table 3. Description of Field Data Used in This Study and the Corresponding References

Property	Symbol	Computation	Units	Number of Sites	RAINFOR Reference
Aboveground biomass	AGB		kg C m^{-2}	69	*Malhi et al*. [2006]
Net primary woody productivity	NPPw		kg C m^{-2} yr^{-1}	25	*Malhi et al*. [2004]
Aboveground biomass change	ΔAGB	=ΔAGB/Δ*t*	kg C m^{-2} yr^{-1}	17	*Baker et al*. [2004]
Fractional aboveground biomass change	fΔAGB	=ΔAGB/AGBo*100	% yr^{-1}	17	*Baker et al*. [2004]
Growth rate	fNPP	=NPPw/AGBo*100	% yr^{-1}	23	*Lewis et al*. [2004c]
Growth rate change	ΔfNPP	=fNPP2 − fNPP1	% yr^{-1}	23	*Lewis et al*. [2004c]
Change in Biomass	ΔAGB pre-2005 and 2005		kg C m^{-2} yr^{-1}	30 pre-2005 13 2005	*Phillips et al*. [2009]

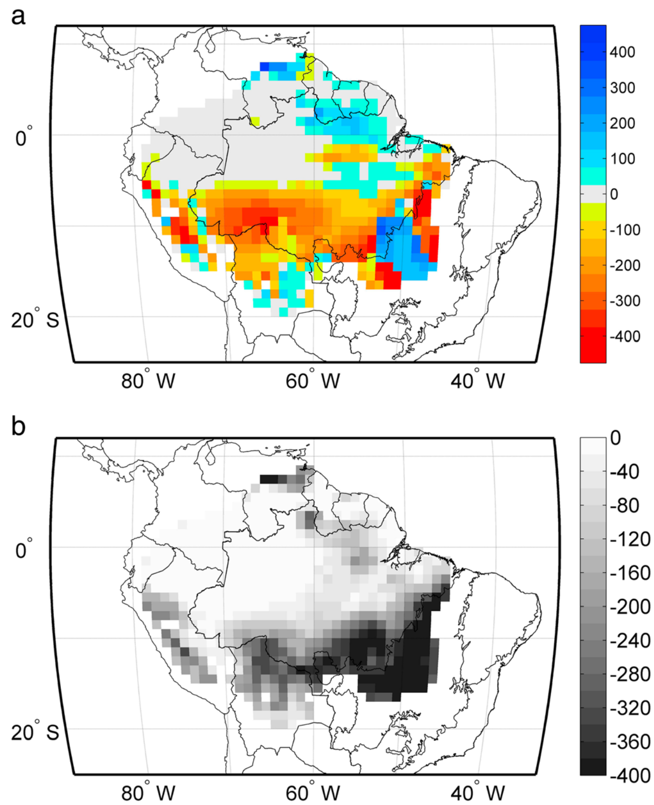

Figure 2. (a) Maximum cumulative water deficit (MCWD) anomaly (mm) for 2005, negative values of MCWD anomaly represent enhanced water stress and positive values represent reduced water stress; (b) mean MCWD (mm) pre-2005.

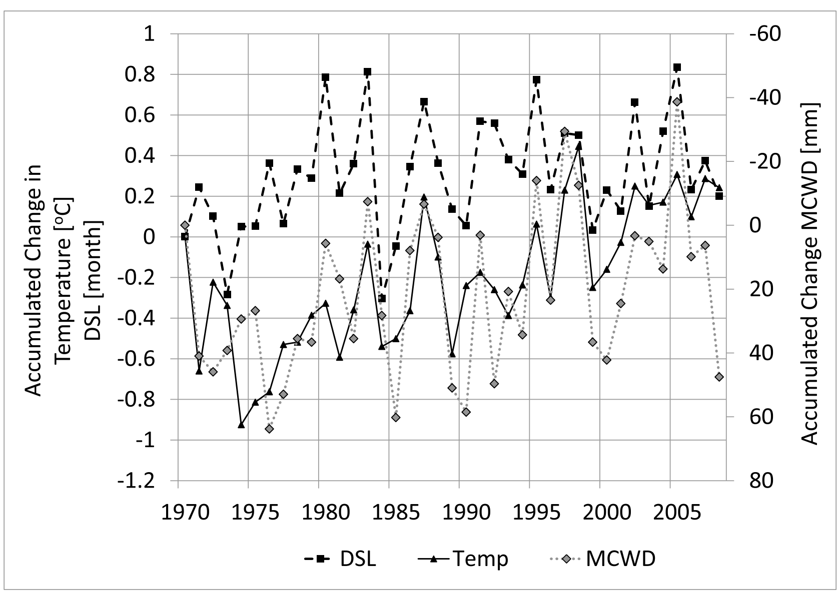

Figure 3. Yearly accumulated changes in temperature (temp), dry season length (DSL), and maximum cumulative water deficit (MCWD) for the time period 1970 to 2008.

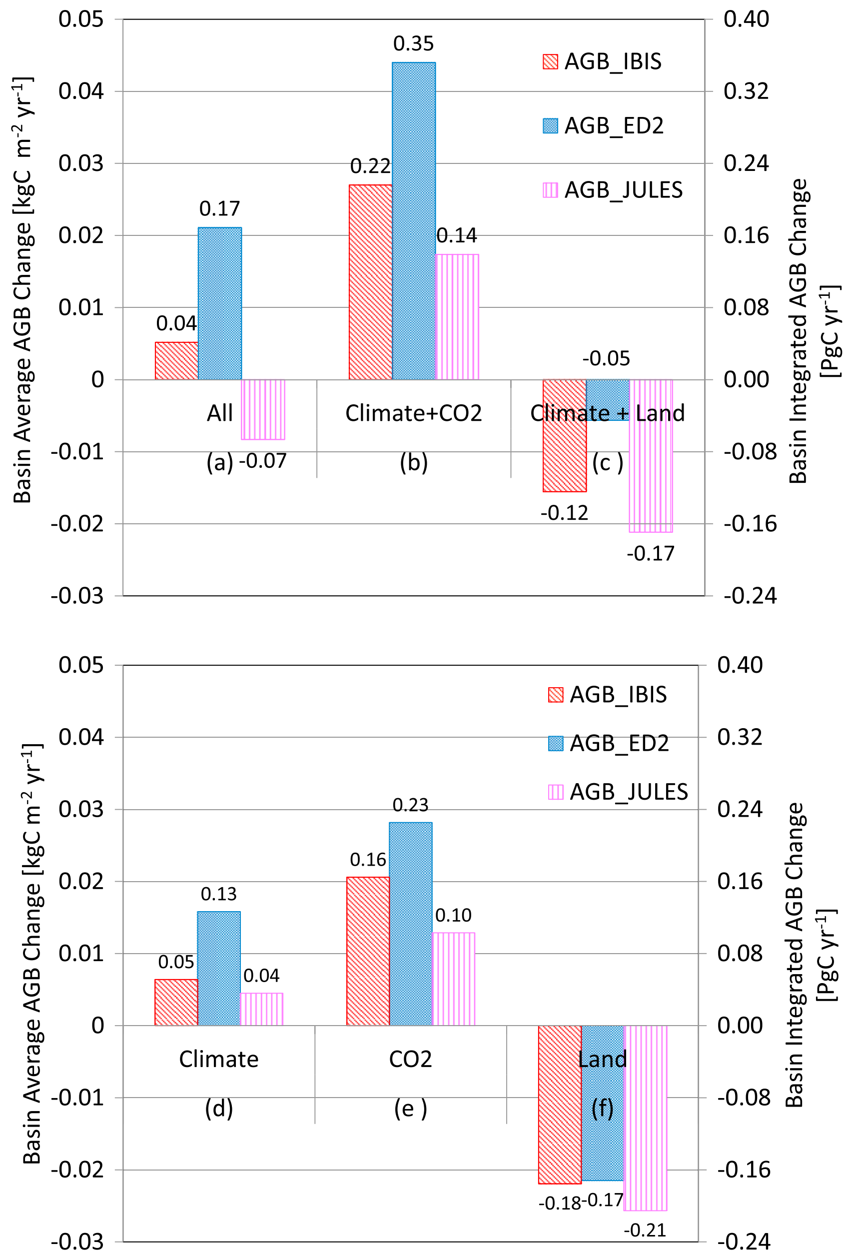

Figure 4. Simulated average (1970–2008) yearly change in aboveground biomass (ΔAGB) for each DGVM (IBIS is in red; ED2 is in blue; JULES is in magenta) and for each forcing combined (a–c) and individually (d–f). The left axis presents the average ΔAGB over the entire study area and time period (kg C m^{-2} yr^{-1}). The right axis presents the time-average ΔAGB integrated over the study area (Pg C yr^{-1}). The numbers shown above the bars represent the corresponding values from the right axis.

census data with a general spatial area of one hectare (see references for more detailed information) and consist of diameter measurements of all individual trees > 10 cm diameter breast high (DBH) within the inventory plots. Repeated censuses allow diameter growth rates of individual trees to be computed. Tree mortality and recruitment are also recorded from census to census. Biomass of individual trees is calculated using the allometric equation of *Chave et al.* [2005] and summed to give total plot-level biomass of trees > 10 cm DBH.

Forest plot data were aggregated to 1° spatial resolution (Figure 1 and Table 3) varying from one to six measurement plots in a grid cell, when available. We compiled published values of aboveground live biomass from 69 grid cells [*Malhi et al.*, 2006]; aboveground woody productivity, 25 gridcells [*Malhi et al.*, 2004];

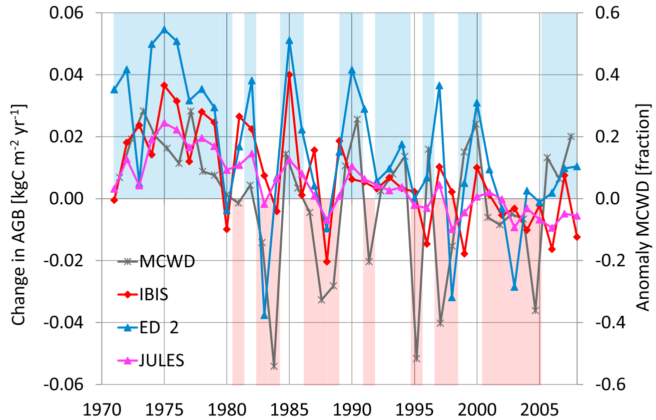

Figure 5. Time series of study area-averaged yearly ΔAGB due to climate effect plus lagged effects of the transient pre 1970 CO_2 increase, (IBIS is in red, ED2 is in blue, and JULES is in magenta), compared to the maximum cumulative water deficit (MCWD) anomaly in gray. Shaded areas in red indicate negative anomalies in MCWD (higher water deficit period), while shaded areas in blue indicate positive anomalies in MCWD (lower water deficit).

changes in aboveground biomass, 17 gridcells [*Baker et al.*, 2004]; and stem growth and mortality rates, 23 sites [*Lewis et al.*, 2004c].

Phillips et al. [2009] analyzed records from long-term plots across Amazonia to assess forest response to the intense 2005 drought relative to pre-2005 conditions. The authors identified increasing biomass before 2005 and a significant reduction in aboveground biomass due to the 2005 drought. We compared this result to the model simulations to assess model sensitivity to extreme drought. The precipitation data used in the model simulations was compared to that used in *Phillips et al*. [2009] and was found to be similar in spatial distribution and magnitude. The 2005 drought year showed a clear increase in water stress (MCWD) in the south and western region of Amazonia (Figure 2a) compared to the average regional water stress, which is concentrated in the southeastern Amazon (Figure 2b).

2.4. Climate Trends in the Studied Period

Here we briefly analyze the main climate trends from the meteorological data used in this study from [*Sheffield et al.*, 2006]. There is a decrease in the temperature from 1970 to the mid-70s followed by an increase until 2008 of about 1°C (Figure 3). This temperature behavior has been identified in other studies as part of a long-term atmospheric oscillation [*Botta et al.*, 2002; *Malhi and Wright*, 2004]. Dry season length (DSL) and maximum cumulative water deficit (MCWD) follow the temperature pattern in the early 70s, with a decrease in the dry season length and water stress followed by an increase in DSL and water stress to the end of the record. The interannual variability of the DSL and MCWD is greater than any net trend along the 39 years of this study, as also observed in previous studies [*Marengo et al.*, 2008]. The climatological data analyses show that except for the first decade (1970–1980), the climate is dominated by interannual variability and not a strong long-term change.

3. Results

3.1. Amazonian Simulation Results 1970–2008

3.1.1. Carbon Balance (1970–2008)

All models simulate an increase in biomass due to increasing atmospheric CO_2 concentrations and climate variations, and a decrease in biomass due to land use change (Figure 4). However, they differ in magnitude depending on their sensitivity to each driver of change. ED2 is clearly the most sensitive to climate and the CO_2 fertilization effect, followed by IBIS, then JULES (Figures 4 and 6).

The combined effects of all factors (climate, CO_2 fertilization, and land use change) from 1970 to 2008 result in a simulated AGB gain with IBIS (0.04 PgC yr^{-1}) and ED2 (0.17 PgC yr^{-1}) and a net loss with JULES (-0.07 PgC yr^{-1}). This represents an annual increase of about 0.08 and 0.25% (in IBIS and ED2, respectively) and a decrease of about 0.05% in JULES, in the integrated AGB across the Amazon basin (Figure 4a). In all models land cover changes impart a decrease in AGB. In IBIS and ED2 the increase in biomass due to climate and CO_2 fertilization

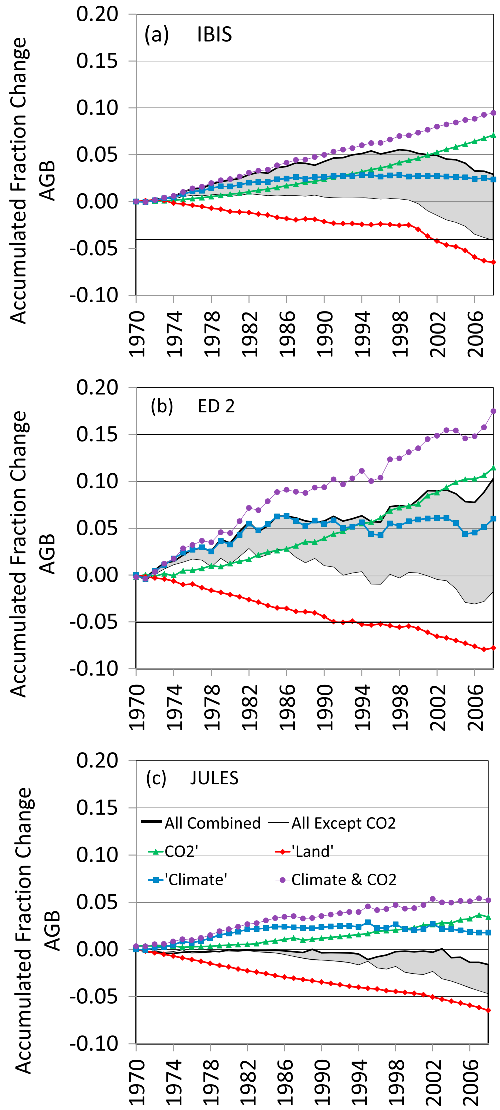

Figure 6. Time series of the fractional aboveground biomass change accumulated from 1970 to 2008 and averaged over the Amazon study area (a) IBIS, (b) ED2, (c) JULES. Each colored line represents the individual effect of climate and lagged CO_2 fertilization effect (blue); CO_2 fertilization (green); land use change (red); and climate and CO_2 fertilization combined (in violet); shaded area represents the maximum net effect considering CO_2 minus the minimum effect not considering the CO_2 fertilization effect. Maps of the fractional accumulated biomass change in 2008 relative to 1970, accounting for (d–f) all forcing, (g–i) climate effect and lagged CO_2 fertilization effect, (j–l) CO_2 fertilization effect only, (m–o) and for land use effect only, for each model, respectively, IBIS, ED2, and JULES. Hot colors indicate increase in biomass and cold colors indicate a decrease in biomass.

(Figure 4b) more than compensates for the loss of biomass due to land use change, while the change simulated by Jules is too small to overcome the AGB loss from land cover (−0.18 in IBIS, −0.17 in ED2, and −0.21 in JULES PgC yr^{-1}, Figure 4f). Although the land use fraction is prescribed for all models, the magnitude of the land use effect differs across models due to differences in background biomass stocks. The CO_2 fertilization effect is the largest contributor to the simulated aboveground biomass increase: 0.16 PgC yr^{-1} for IBIS (77% of change), 0.23 PgC yr^{-1} for ED2 (63% of change), and 0.10 PgC yr^{-1} for JULES (77% of change), respectively (Figure 4e) in the last 39 years (1970–2008). Without the CO_2 fertilization effect all models would have simulated a net forest biomass loss during the simulation period (Figure 4c). Climate combined to the lagging effect after freezing CO_2 to constant levels contributed to a small increase in AGB of 0.05 (IBIS), 0.13 (ED2), and 0.04 (JULES) PgC yr^{-1} (Figure 4d).

The relative importance of different drivers of change varies in time and space (Figures 5 and 6). Although CO_2 fertilization exerted the strongest influence on the C balance in the long term, much of the interannual variability in C balance was governed by variability in climate. There was little evidence of a trend in climate during the simulation period (Figure 3), but interannual variations were large and important where changes in biomass ranged from plus or minus 0.04 kgC m^{-2} yr^{-1} (Figure 5) 3 times larger than the mean annual climate effect (Figure 4d).

Temporal patterns of ΔAGB were found to be closely related to patterns of background MCWD (Figure 5). Extreme climate events such as El Niño in 1983 and 1998 and the warm north tropical Atlantic in 2005 are distinguishable in the MCWD, and result in simulated biomass decrease (Figure 5, red shaded areas). More favorable climate periods, particularly during the 1970s, result in an increase in biomass (Figure 5, blue areas). Simulated biomass change was shown to be sensitive to climatic interannual variability by all models, with higher sensitivity in ED2 model.

In the first decade (1970–1980) climate changes plus the CO_2 lagging effect resulted in a simulated increase in biomass by all models. ED2 was most sensitive (0.5% yr^{-1} biomass increase), while IBIS and JULES were about half as sensitive (0.25% yr^{-1} biomass increase) (Figure 6a). After 1980 the climate effect contributed to a null up to a slight decrease in change in simulated cumulative AGB at the end of the period, in all models (Figure 6a).

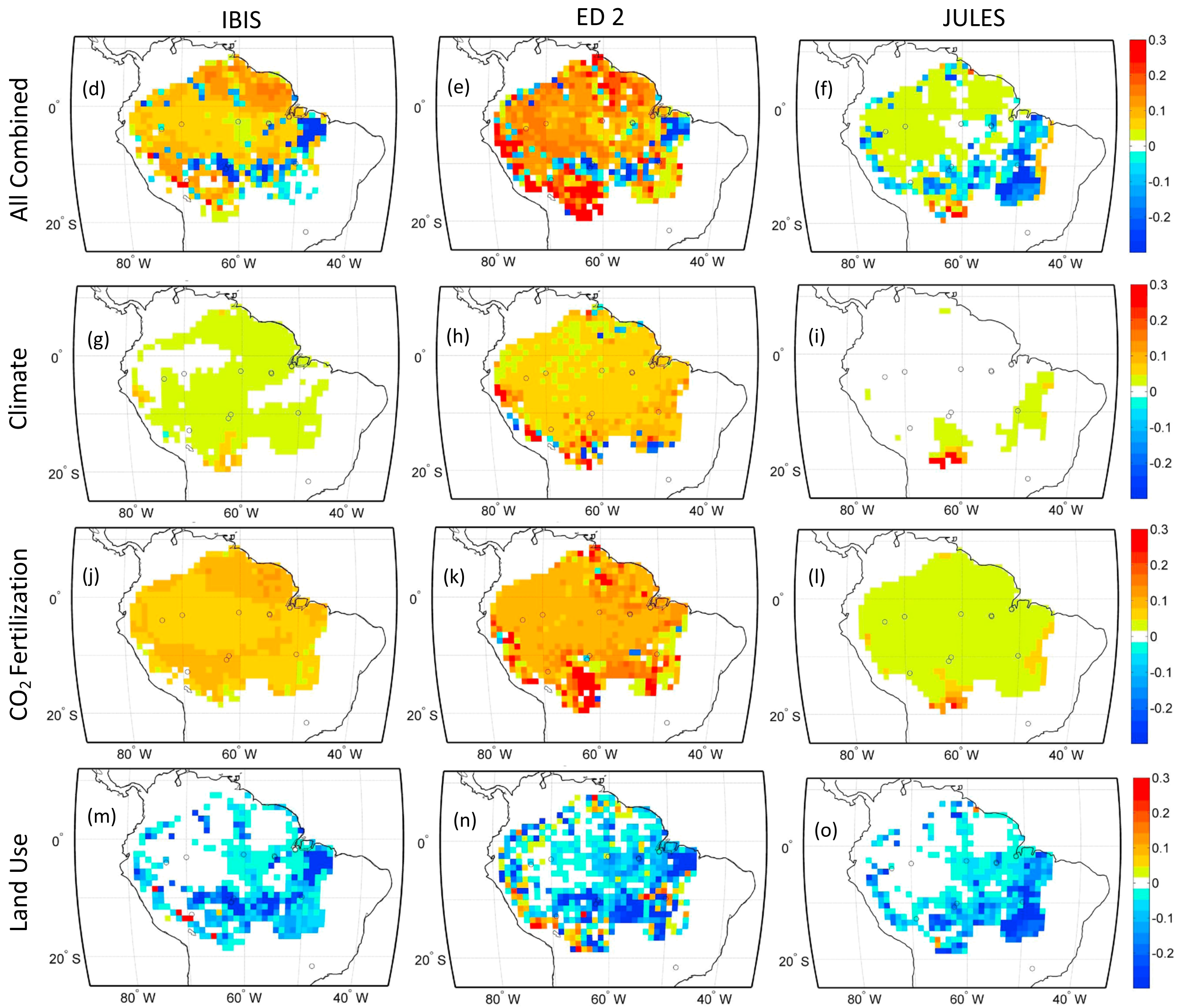

Figure 6. (continued)

The analysis also revealed interesting temporal (Figures 6a–6c) and spatial patterns (Figures 6d–6o) in biomass gains/losses. While the CO_2 fertilization effect is more apparent in the long term analyses, the climate effect tends to zero in the long term. The opposite effect is noticed in the short term. This happens because the CO_2 fertilization effect is a positive and cumulative effect while the climatic effect varies considerably on an inter-annual basis.

Land use change is clearly the most important single-factor driving spatial variability in AGB change in the studied period of time (Figures 6m–6o), being most pronounced in the southern, southeastern part of the Amazonian study area. Climate and CO_2 effects made modest contributions to the spatial variability (Figures 6g–6i). There was evidence in our simulations that the strength of the climate and CO_2 effects also varied in different parts of the Amazon. In all models, climate-driven gains in biomass were strongest in the

Table 4. Mean (and Standard Deviation) AGB Stocks and NPP_W Across Field Measurement Sites and Corresponding Time Period [*Malhi et al.*, 2006, 2004] and as Simulated by Each Numerical Model

	Field Observation	IBIS	ED2	JULES	IBIS-HP
AGB [kg C m^{-2}]	14.8(2.7)	11.3(2.3)	11.0(4.2)	14.6(2.0)	13.7(2.3)
NPPw [kg C m^{-2} yr^{-1}]	0.29(0.07)	0.66(0.06)	0.46(0.22)	0.42(0.20)	0.34(0.04)

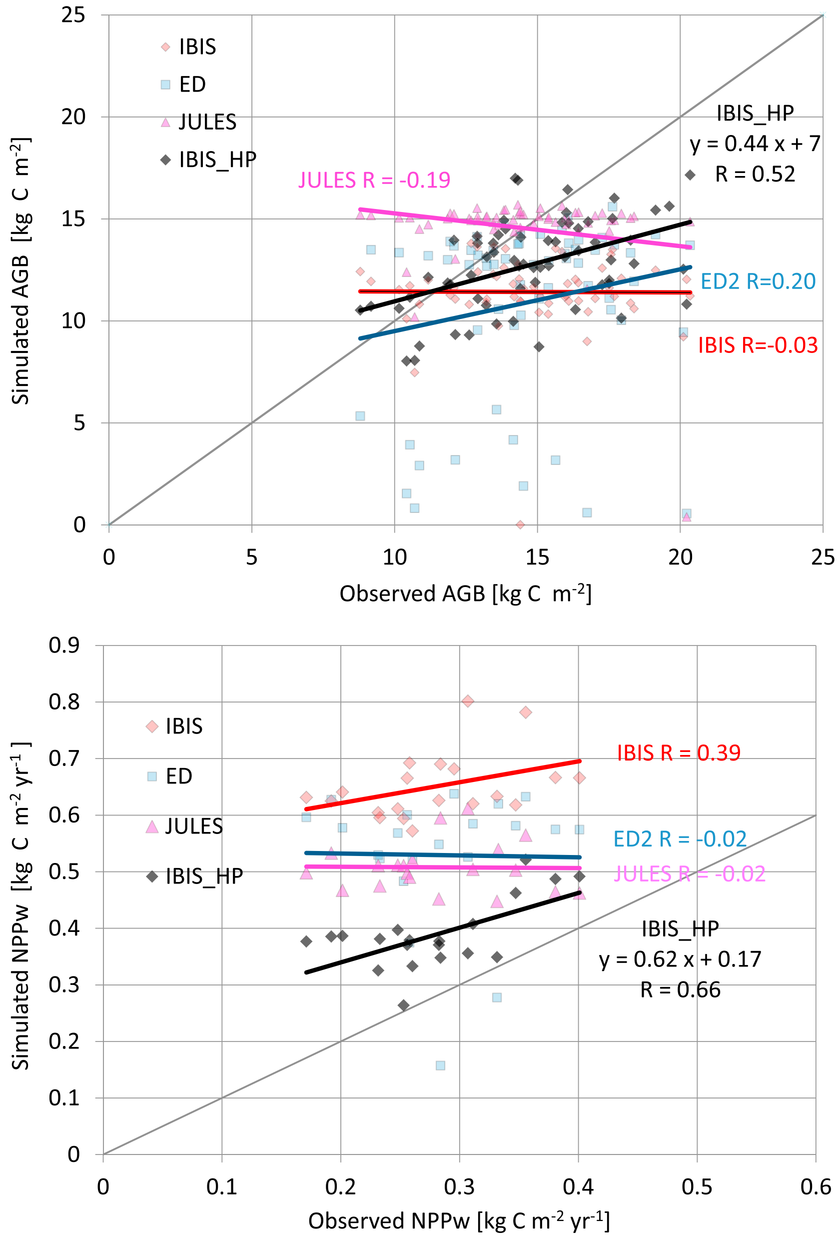

Figure 7. (a) Simulated AGB compared to field estimates from *Malhi et al.* [2006]; (b) Simulated NPP_w compared to field estimates from *Malhi et al.* [2004]. The model simulations are IBIS (red), ED2 (blue), JULES (magenta), and IBIS HP (black), for periods of time and location corresponding to the field measurements.

southwestern edge of the Amazon. ED2 simulated climate-driven declines in biomass in southeastern Amazon that were not simulated by IBIS or JULES. ED2 and JULES also simulated strong positive CO_2 effects in the southwestern Amazon, in contrast to IBIS, which simulated a weaker response of biomass to CO_2 in the southwestern Amazon than in the remainder of the study area. These results are consistent with a stronger water use efficiency response under high CO_2 over drier regions of the Amazon in JULES and ED2 than in IBIS.

3.2. Forest Plot Data-Model Comparison

3.2.1. Evaluation of Spatial Patterns of AGB and NPP_w

Mean simulated aboveground biomass (AGB) values across the study area are within the range of the observations, while NPP_w is systematically overestimated (Table 4). All DGVMs simulated a spatially homogeneous distribution of biomass and productivity, in contrast to the field observations that show a strong variability

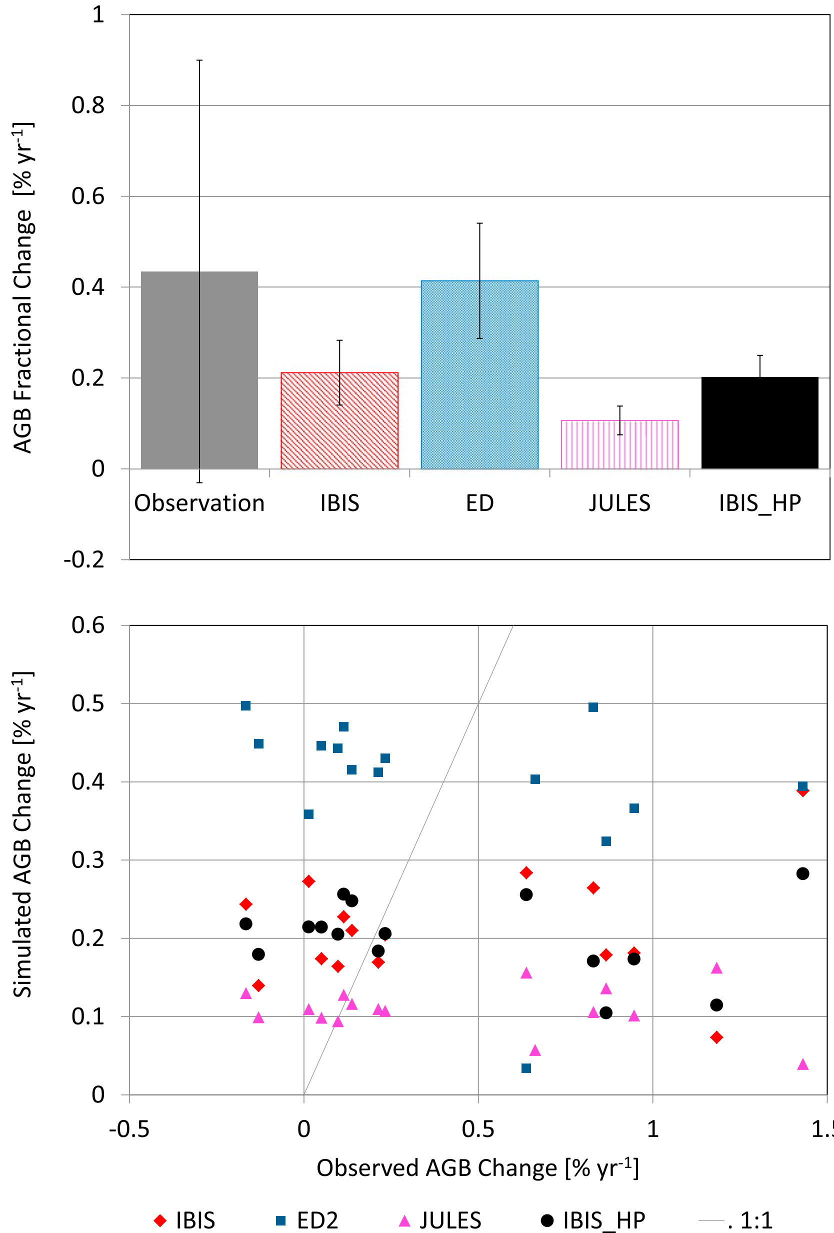

Figure 8. Fractional AGB change (f∆AGB) simulated by each model compared to f∆AGB from field observations, for periods of time and location corresponding to the field measurements: IBIS (red), ED2 (blue), JULES (magenta), IBIS_HP (black). (a) Bar plot representing the average over the corresponding field sites locations; error bars represent the standard deviation between the sites. (b) Scatter plot comparing simulated to observed estimates by field site.

across the study area (Figure 7). Field data suggest a gradient of lower AGB stock and higher productivity in western and southern Amazonia and a higher biomass stock and lower productivity in central Amazonia (AGB ranging from 9 to 20 kg C m^{-2} and productivity ranging from 0.15 to 0.55 kg C m^{-2} yr^{-1}) [*Malhi et al.*, 2006, 2004]. The spatial variability of estimates of AGB and NPP_w has been shown by *Castanho et al.* [2013] to be strongly related to the spatial heterogeneity of woody residence time and soil fertility, which are included in IBIS_HP but not in the other models.

The IBIS-HP results, which explicitly include spatially heterogeneous parameterization, are presented for comparison (Figure 7, black dots). The IBIS-HP results indicate that consideration of the spatial heterogeneity of the key model parameters is crucial for capturing the spatial variability of AGB and NPPw observed from field

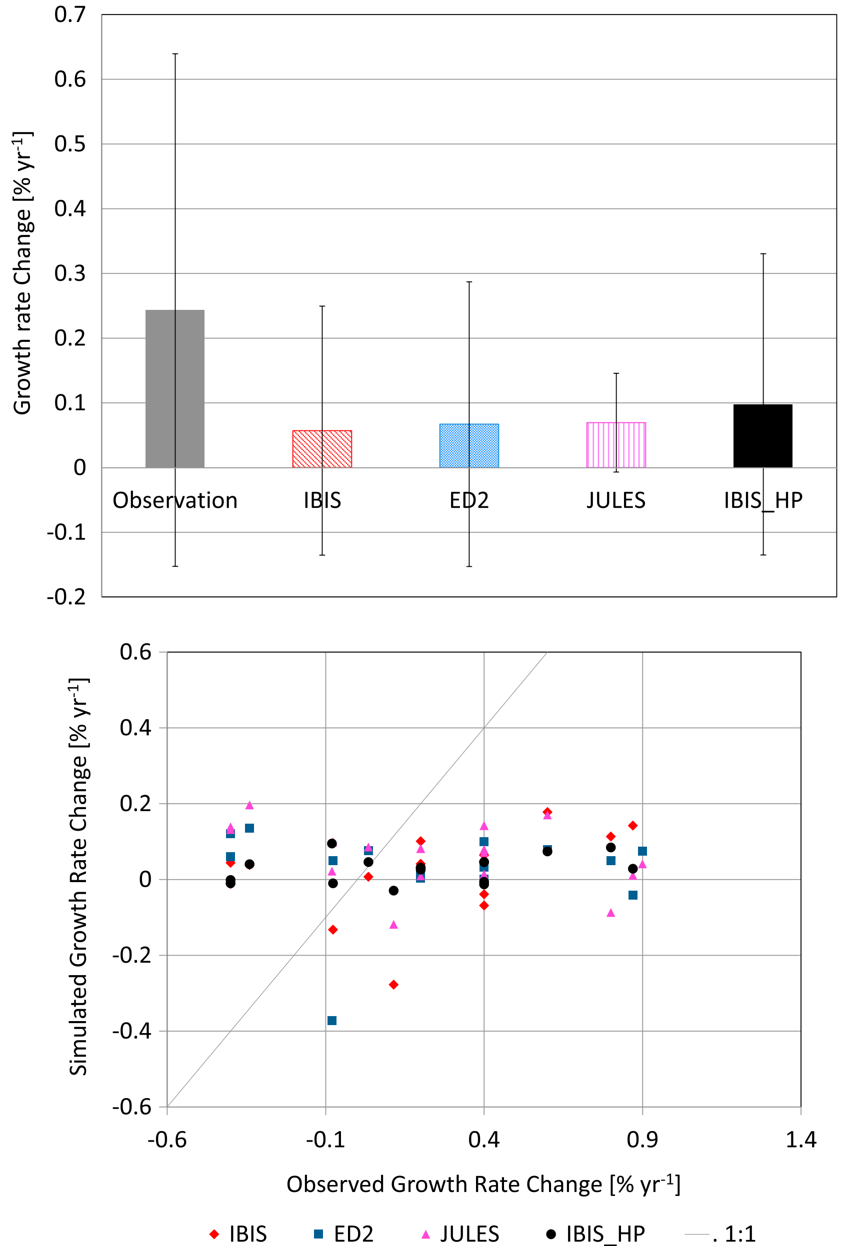

Figure 9. Growth rate change ($\Delta fNPP_w$) simulated by each model compared to field observations, for periods of time and location corresponding to the field measurements: IBIS (red), ED2 (blue), JULES (magenta), IBIS_HP (in black). (a) Bar plot representing the average over the corresponding field sites, and (b) scatter plot comparing simulated to observed estimates by field site.

data [*Castanho et al.*, 2013]. The average of simulated AGB across the measurement sites is close to that of the field observations of AGB (13.7(2.3) and 14.8(2.7), IBIS-HP and field observations, respectively) (Table 4). The NPP_w simulated by all models is systematically overestimated compared to the observations. This overestimation is related to the way the models allocate the NPP between the plant compartments, overestimating the allocation to wood [*Castanho et al.*, 2013]. Correcting for this bias in the IBIS-HP simulation results in a better representation of NPP_w compared to field estimates (0.34(0.04) versus 0.29(0.07) respectively).

3.2.2. Evaluation of Simulated AGB Change (ΔAGB) and NPP_w Change (ΔNPP_w) With Forest Plot-Based Estimates

Estimates based on field data plots show an average ΔAGB of 0.062(0.083) kgC m^{-2} yr^{-1}[*Baker et al.*, 2004; *Lewis et al.*, 2004a, 2004c; *Phillips et al.*, 1998]. The plots in these analyses are located in old growth forests and are not

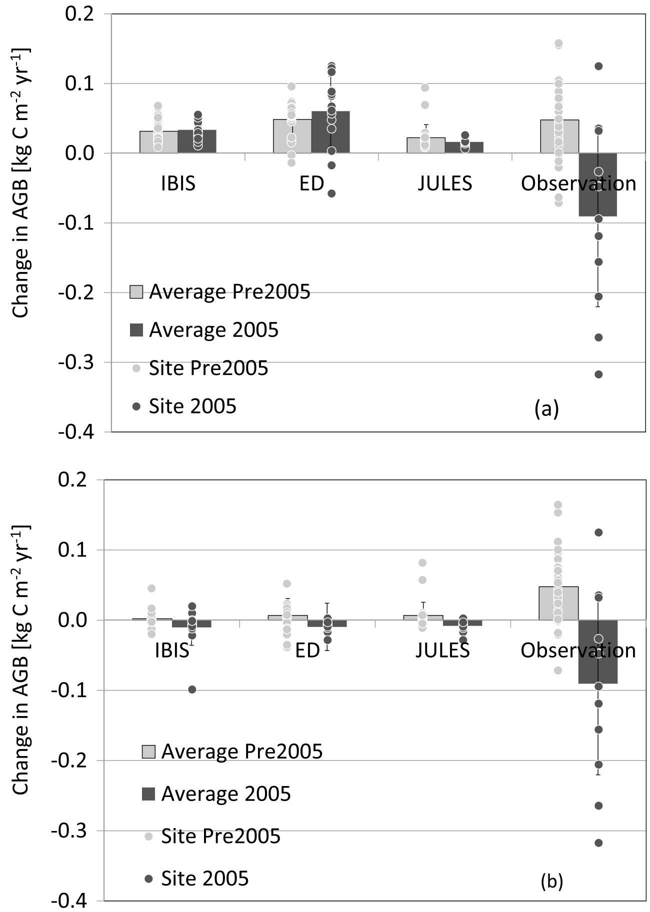

Figure 10. Simulated and observed ΔAGB averaged over the sites of analyses. Gray bars represent the pre-2005 period and black bars represent the 2005 drought period. Gray and black dots show individual site-level data for pre-2005 and 2005 periods, respectively. (a) Simulated results with the combined effect of Climate and CO_2 fertilization effects; (b) Simulated results of climate effect and lagged pre1970 CO_2 increase effects only. Field data observations were adapted from *Phillips et al*. [2009].

affected by land use change. We compared ΔAGB from field data sites to the simulated values of corresponding grid cells, accounting for climate and CO_2 forcing only (excluding land use change). The mean simulated ΔAGB was net positive for all models (+0.03 ± 0.01 kg C m^2 yr^{-1} for IBIS, +0.017 ± 0.005 kg C m^2 yr^{-1} for JULES to +0.04 ± 0.01 kg C m^2 yr^{-1} for ED2). ED2 simulated the highest mean fΔAGB and was the closest to the mean fΔAGB across the forest inventory plots (Figure 8a). All three models have very low spatial variability in fΔAGB compared to the field observations (Figure 8b).

Simulated $\Delta fNPP_w$ varies considerably among the DGVMs and none compare well with the observations [*Lewis et al*., 2004a] (Figure 9). Although IBIS_HP simulates AGB and NPP_w values that are in better agreement with the observations than the other models, the simulated fΔAGB and $\Delta fNPP_w$ is poor (Figure 8, Figure 9). Thus, none of the models, whether big-leaf or stand-level architecture, capture plot-specific biomass dynamics. The hypotheses for this response are explored in the discussion section.

3.2.3. Evaluation of Simulated AGB Response to the 2005 Drought

In a manner analogous to the study of *Phillips et al*. [2009], we compare average annual ΔAGB for observations (specific field plots) and models before the 2005 drought event to ΔAGB during the 2005 drought year. Output from simulations considering only CO_2 and climate are used for this analysis. Mean-simulated ΔAGB (Figure 10a, gray bars) pre-2005 is similar to that presented in Figure 4a, for the entire study area. All models simulate pre-2005 ΔAGB lower or close to observations, despite failing to capture the observed spatial variability (Figure 10a, gray dots). The field data indicates a decrease in biomass (negative ΔAGB) in most of the sites in 2005 drought compared to an increase in biomass pre-2005.

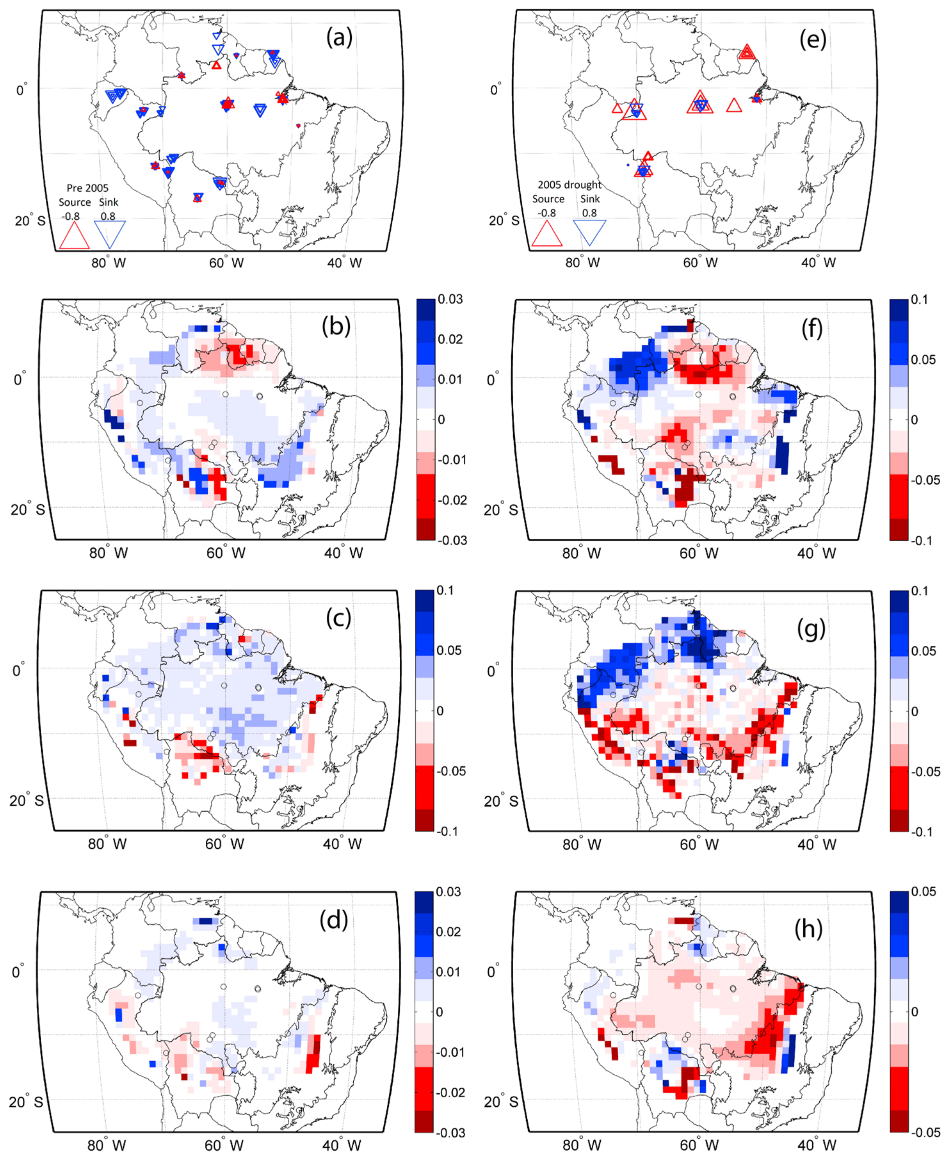

Figure 11. Aboveground biomass change (kg Cm^{-2} yr^{-1}) pre-2005: of (a) field observations, from model simulation with climate only effect (e, b, and f) for IBIS, ED2, and JULES, respectively. Aboveground biomass change (kg Cm^{-2} yr^{-1}) 2005 drought of (c) field observations, form model simulation with climate only effect (g, d, and h) for IBIS, ED2, and JULES, respectively. (Figures 11a–11d) An overall sink of C (blue) with a positive AGB change in the decadal pre-2005 period. (Figures 11e–11h) The 2005 drought year with a negative AGB and most of the study area being a source of carbon (red).

Analysis of simulations without increasing CO_2 (climate only) shows that despite underestimating ΔAGB compared to field results, models are able to distinguish between pre-2005 increases in biomass and decreases in biomass in 2005 due to the drought stress in many sites (Figure 10b). However, the modeled reduction in ΔAGB due to climate is insufficient to reverse the sign of the change due to CO_2 fertilization and all models suggest that the Amazon continues to be a carbon sink during the 2005 drought (Figure 10a, black bars).

The spatial distribution of simulated ΔAGB, with climate effect only, in the pre-2005 period in most regions is a positive (Figures 11a–11d, blue/sink) for all models in qualitative agreement with the observations, but the models underestimate the magnitude. During the 2005 drought period (Figures 11e–11h, red/source) model and field data show an overall decrease in biomass with isolated areas of increasing in biomass.

4. Discussion and Conclusions

4.1. Drivers of Amazon Carbon Balance

This study quantified the importance of the major drivers of variability of the Amazonian carbon balance from 1970 to 2008. Whereas attribution of change is difficult from analysis of the field data alone, models allow for clear separation of the importance of individual factors. The main factors analyzed were CO_2 fertilization, climate, and land use change.

In undisturbed forest areas, the DGVMs analyzed here agree with forest inventory observations that above ground biomass has increased across Amazonia over the last years [*Baker et al.*, 2004; *Lewis et al.*, 2004b, 2004c; *Phillips et al.*, 1998]. Our factorial analysis suggests that the CO_2 fertilization effect is the major factor responsible for the simulated historical increase in AGB (Figure 4e). The climate in the period showed no specific trend resulting in a close to null contribution in the integrated time; however, it does affect biomass at the interannual scale.

Land use change was shown to be of great importance for the regional carbon budget, being similar in magnitude to the CO_2 fertilization effect (Figure 4f). In IBIS and ED2, biomass losses due to land use change, although significant, were insufficient to negate CO_2 gains, resulting in an overall gain of biomass over Amazonia over the simulation period. In the JULES simulations, biomass losses resulting from land use change outweighed biomass gains due to climate and CO_2 fertilization, resulting in a net loss of biomass over Amazonia over the simulation period. The regional patterns of biomass change closely follow those of deforestation, with biomass decreases concentrated in the eastern and southern margins of the regions (Figure 6). Areas subject to less deforestation in central and western Amazonia generally gained biomass. The source of carbon due to deforestation found in this study (-0.18 in IBIS, -0.17 in ED2, -0.21 in JULES $PgC\,yr^{-1}$, Figure 4f) is well within the estimates in other works. *Aragão et al.* [2014] estimate a carbon source due to gross deforestation ranging from -0.12 to $-0.23\,PgC\,yr^{-1}$, simulations with LPJmL resulted in -0.17 to $-0.22\,PgC\,yr^{-1}$ [*Poulter et al.*, 2010].

The magnitude of the biomass changes simulated by the models is broadly in agreement with bottom up studies, usually based on book-keeping methods. IBIS and ED reported a mean regional sink of 0.04 and $0.17\,PgC\,yr^{-1}$ (Amazonia-South America Tropical Forest $8 \cdot 10^6\,km^2$ 1970–2008) when all factors were considered while JULES simulated a net biomass source of $0.07\,PgC\,yr^{-1}$ over the simulation period (Figure 4a). Bottom up analyses from *Pan et al.* [2011], using forest inventory data and long-term ecosystem C studies, suggested a C sink of $0.07\,PgC\,yr^{-1}$ (Tropical America, 2000–2007). *Malhi* [2010] estimated a net sink of C of $0.03 \pm 0.15\,PgC\,yr^{-1}$ which they concluded was not significantly different from zero (Tropical Americas $8.02 \cdot 10^6\,km^2$, 2000–2005). *Aragão et al.* [2014] estimated a current net carbon sink in 2010 for Brazilian Amazonia on the order of $0.16\,PgC\,yr^{-1}$ (ranging from sink 0.11 to sink $0.21\,PgC\,yr^{-1}$); however, the authors state that this value can be a source in drought years of $0.06\,PgC\,yr^{-1}$ (ranging from source 0.01 to source $0.31\,PgC\,yr^{-1}$). The net balance simulated by the models in this study as well as the estimates in literature suggest a null to an average sink of carbon in the Amazon in the last decades. The models also indicate that there is a significant interannual variability whereby the carbon balance can fluctuate between a sink and a source of carbon, as well as observed in [*Gatti et al.*, 2014] driven primarily by extreme climate events and the processes that occur with them. Therefore, future climate, atmospheric CO_2 concentration, frequency of extreme climatic events, as well as the intensity of fires [*Balch et al.*, 2015; *Brando et al.*, 2014], and the rates of deforestation will all be key factors in determining the contribution of the Amazonian forest to the global C balance.

Our results have clear implications for studies focusing on the future carbon balance of Amazonia. Recent studies involving simulations of DGVMs with ensembles of climate model forcings have suggested an overall resilience of Amazonian forests to climate change [e.g., *Huntingford et al.*, 2013; *Rammig et al.*, 2010]. However, such studies generally do not take into account land use change or accurate estimates due to fire. Persistent future deforestation may effectively cancel or reverse the significant land sink predicted by many models in the future [*Zhang et al.*, 2015].

Despite the advances made in this study, it is important to acknowledge that the current structure of the DGVMs used in this study has prevented assessment of some potential mechanisms that may contribute to Amazonian biomass dynamics [*Coe et al.*, 2013]. In addition to climatic factors (e.g., changing rainfall, temperature, and radiation patterns) and increasing CO_2, increasing nutrient deposition, especially nitrogen and phosphorus, from biomass burning and also long-range transport of Saharan dust, have been considered as potential agents of dynamic change in Amazonian forests [*Lewis et al.*, 2009]. However, the lack of fully interactive nitrogen and phosphorus cycles in the models used in this study precludes assessment of the role of nutrient deposition on the Amazonian C balance. It has also been proposed that the increasing biomass storage in Amazonian rainforests reflects recovery from large-scale disturbance events [e.g., *Wright*, 2005]. However, large disturbances such as blow down events are not really considered in the current simulations. Finally, an increase in liana abundance over time has been reported in Amazonia [*Phillips et al*., 2002]. Lianas are thought to be favored by increasing atmospheric CO_2 and can alter forest structure by increasing tree mortality [*Van Der Heijden et al*., 2013].

4.2. Sensitivity to Extreme Events

Extreme climatic events play an important role in the global carbon cycle [*Reichstein et al*., 2013]. Although the latest evidence suggests that the global land carbon sink continues to increase [*Le Quere et al*., 2009], its interannual variability is linked to extreme climatic events. For example, *Zscheischler et al*. [2014] recently showed that extreme events, mainly linked to drought, dominate the global interannual variability in gross primary productivity (GPP). Thus, accurate modeling of the impacts of extreme events is essential for reliable predictions of climate impacts on global ecosystems.

The Amazon region has experienced a number of extreme drought events in recent decades. These include the El-Nino–Southern Oscillation (ENSO) events of 1982/1983, 1986/1987, and 1997/1998 as well as the recent droughts of 2005 and 2010, which were associated with large, positive north Atlantic sea surface temperature anomalies, with a different spatial fingerprint to ENSO droughts. We found that the three DGVMs evaluated in this study were unable to reproduce the biomass losses observed in forest inventory data across Amazonia following the 2005 drought event in Amazonia. This was not an artifact of the forcing climate data, which adequately captured patterns of rainfall anomalies, but a result of the insensitivity of simulated biomass to drought conditions. This result is consistent with previous studies that show that models are not able to capture the response of forests to imposed experimental drought, greatly underestimating biomass loss [*Galbraith et al*., 2010; *Powell et al*., 2013; *Sakaguchi et al*., 2011]. These studies have shown that while simulated carbon fluxes such as gross primary productivity (GPP) and net primary productivity (NPP) may have large reductions during drought, the effect on simulated carbon stocks is minimal. The lack of biomass response to drought is likely related to the inadequate representation of forest carbon turnover and mortality in these models [*Galbraith et al*., 2013], emphasizing the need for a revised treatment of drought-induced mortality in DGVMs. As shown by *Powell et al*. [2013], our analysis also finds that ED2 is the most sensitive model to drought in terms of its biomass response. Field experiments of rain exclusion and observations of interannual variability have helped provide a better understanding of the tropical forest behavior to drought stress. Empirical and mechanistic formulations have been developed to characterize tropical forest tree mortality in response to water stress [*Brando et al*., 2012; *Phillips et al*., 2009; *Powell et al*., 2013] but have not been incorporated in numerical models yet.

The insensitivity of DGVMs to extreme natural drought events such as the 2005 Amazonian drought event has significant implications. The study area average simulated carbon fluxes responded to interannual variability of climate reasonably well (Figure 5). However, the mechanisms involved in the response of vegetation to interannual variations in temperature and rainfall are fundamentally different to those involved in the response to extreme events. Responses of vegetation to interannual variation in climate are dominated by the response of photosynthetic and respiratory fluxes, which DGVMs include. On the other hand, responses to extreme events, as shown by *Phillips et al*. [2009] for the 2005 Amazonian drought, are dominated by tree mortality processes, which these DGVMs do not yet incorporate.

4.3. Spatial Patterns of Stock and Biomass Change

In agreement with previous studies [*Delbart et al*., 2010], we found that none of models in this study, except for IBIS_HP as highlighted by *Castanho et al*. [2013], are able to reproduce observed spatial gradients in biomass and productivity across Amazonia. This stems from a number of model structural deficiencies, including the lack of interactive cycling of phosphorus, an important determinant of forest structure and productivity in Amazonia [*Quesada et al*., 2012] as well as the lack of mechanistic treatment of carbon turnover processes [*Galbraith et al*., 2013] and simplistic descriptions of carbon allocation [*Malhi et al*., 2011].

Increasing CO_2 led to increased biomass gains across the entire Amazon region, with relative increases appearing to be greater in the drier southern region of the Amazon, especially in ED2 and JULES. This may be linked to increased water use efficiency under higher CO_2, an effect that would have greater benefit in drier environments. Observational data on water use efficiency is rare for tropical forests, but some evidence of increasing water use

Table A1. The Canopy Physiological Processes Governing Plant Photosynthesis and How They Control Water and CO_2 Fluxes in the Vegetation Canopy for Each of the Numerical Models are Described in Detail

	IBIS [*Foley et al.*, 1996; *Kucharik et al.*, 2000]	ED2 [*Medvigy et al.*, 2009; *Moorcroft et al.*, 2001]	JULES [*Best et al.*, 2011; *Clark et al.*, 2011; *Cox et al.*, 1998]
[*Collatz et al.*, 1991; *Farquhar et al.*, 1980]	C3 photosynthesis is expressed as the minimum of three potential capacities to fix carbon similarly in all models as follows		
A_g (mol CO_2 m^{-2} s^{-1}), gross Photosynthesis rate per unit leaf area	$A_g \cong \min(J_e, J_c, J_s)$		
A_n (mol CO_2 m^{-2} s^{-1}), net leaf assimilation rate	$A_n = A_g - R_{leaf}$	$A_o = A_g - R_{leaf}$ open stomata $A_c = -R_{leaf}$ closed stomata $A_n = \text{stressf}A_o + (1 - \text{stressf})A_c$	$A_n = (A_g - R_{leaf})\text{stressf}$
R_{leaf} (mol CO_2 m^{-2} s^{-1})	$R_{leaf} = \gamma V_{max}$ where γ is the leaf respiration cost of Rubisco activity [*Collatz et al.*, 1991]		
J_e (mol CO_2 m^{-2} s^{-1}), light-limited rate of photosynthesis	$J_e = \alpha \text{PAR}_l \frac{C_i - \Gamma}{C_i + 2\Gamma}$ where *a* is quantum efficiency, PAR_l is the photosynthetically active radiation absorbed by the vegetation layer (*l*), C_i is the leaf intracellular CO_2 concentration and Γ is the compensation point for gross photosynthesis		
J_c (mol CO_2 m^{-2} s^{-1}), Rubisco limited rate of photosynthesis	$J_c = V_{max}\left(\frac{C_i - \Gamma}{C_i + K_c(1 + [O_2]/K_o)}\right)$ where V_{max} is the maximum capacity of Rubisco (mol CO_2 m^{-2} s^{-1}), K_c and K_o (mol mol^{-1}) are the Michaelis-Menten parameters for CO_2 and oxygen, respectively		
J_s (mol CO_2 m^{-2} s^{-1}), photosynthesis is limited by the inadequate rate of utilization of triose phosphate, "sucrose synthesis limited," $J_s = V_{max}/2.2$	$J_s = 3\frac{V_m}{8.2}\left(1 - \frac{\Gamma}{C_i}\right) + \frac{J_p\Gamma}{C_i}$ $J_s = \frac{V_{max}}{2.2}$	-x-	$J_s = \frac{V_{max}}{2}$
A_g (mol CO_2 m^{-2} s^{-1}), gross Photosynthesis rate per unit leaf area	$\theta J_p^2 - J_p(J_e + J_c) + J_e J_c = 0$ $\beta A_g^2 - A_g(J_p + J_s) + J_p J_s = 0$ where $\theta = 0.9$ and $\beta = 0.9$ are empirical constants governing the sharpness of the transition between the three potential photosynthesis		$\theta J_p^2 - J_p(J_e + J_c) + J_e J_c = 0$ $\beta A_g^2 - A_g(J_p + J_s) + J_p J_s = 0$ where $\theta = 0.83$ and $\beta = 0.93$ are empirical constants governing the sharpness of the transition between the three potential photosynthesis
Γ (mol mol^{-1}) compensation point for gross photosynthesis	$\Gamma = \frac{[O_2]}{2\tau}$ $\Gamma = 2.3\ 10^{-5}\ \exp\left[4500\left(\frac{1}{288.15} - \frac{1}{T}\right)\right]$ where O_2 is the atmospheric oxygen concentration and *t* is the ratio of kinetic parameter describing the partitioning of enzyme activity to carboxylase or oxygenase function	$\Gamma = (21.2\ \text{ppmv})\ \exp\left[5000\left(\frac{1}{288.15} - \frac{1}{T}\right)\right]$ where *T* is ambient temperature	$\Gamma = \frac{[O_2]}{2\tau}$ where $\tau = 2600\ Q_{10\_rs}^{0.1(T_c - 25)}$ with $Q_{10\_rs} = 0.57$.

10.1002/2015GB005135

Table A1. (continued)

	IBIS [*Foley et al.*, 1996; *Kucharik et al.*, 2000]	ED2 [*Medvigy et al.*, 2009; *Moorcroft et al.*, 2001]	JULES [*Best et al.*, 2011; *Clark et al.*, 2011; *Cox et al.*, 1998]
V_{max} (mol CO_2 m^{-2} s^{-1}), maximum capacity of Rubisco enzyme	The V_{max} is an exponential function of temperature and it applies a phenomenological cut off for very low or very high temperatures (278.16 K and 323.16 K, respectively) ($f(T_{leaf})$). It is also modulated by a water stress factor based on plant available soil moisture (stressf) $V_{max} = V_m * f(T_{leaf}) * \text{stressf}$ where V_m is prescribed as a function of the PFT	The V_{max} is an exponential function of temperature and it applies a phenomenological cut off for very low or very high temperatures (T_o and 318.15 K, respectively) ($f(T_{leaf})$). It is also ramps down photosynthesis in the fall ($e(t)$) $V_{max} = V_m * f(T_{leaf}) * e(t)$	The V_{max} is an exponential function of temperature and it applies a phenomenological cut off for very low or very high temperatures (T_{low} and T_{up}, respectively) ($f(T_{leaf})$) $V_{max} = V_m * f(T_{leaf})$
$f(T_{leaf})$, modulate photosynthesis through modifying V_{max} by phenomenological as a function of temperature	$f(T_{leaf}) = \frac{\exp 3500 * \left(\frac{1}{288.18} - \frac{1}{T_{leaf}}\right)}{(1+\exp 0.4(278.16 - T_{leaf}))(1+\exp(0.4(T_{leaf} - 323.16))}$	$f(T_{leaf}) = \frac{\exp 3000 * \left(\frac{1}{288.15} - \frac{1}{T_{leaf}}\right)}{(1+\exp 0.4(T_o - T_{leaf}))(1+\exp(0.4(T_{leaf} - 318.15))}$	$f(T_{leaf}) = \frac{\exp 3500 * \left(\frac{1}{288.18} - \frac{1}{T_{leaf}}\right)}{(1+\exp 0.3(T_{low} - T_{leaf}))(1+\exp(0.3(T_{leaf} - T_{up}))}$
Stressf, modulate photosynthesis by stress factor based on soil moisture	$\text{stressf} = \frac{1-\exp(-5)\frac{(\theta-\theta_{wilt})}{(1-\theta_{wilt})}}{1-\exp(-5)}$ where θ is the soil moisture content and θ_{wilt} is the soil wilting point; the stress factor ranges from 1 ($\theta = 1.0$) and 0.0 ($\theta = \theta_{wilt}$), applied over the V_{max}	$\text{stressf} = \frac{1}{1+\frac{\text{Demand}}{\text{Supply}}}$ where $\text{Demand} = ET_{max} SLA\, B_{leaf}$ $\text{Supply} = K_w \theta B_{root}$	A_n* stressf $\text{stressf} \begin{cases} 1 \; for \; \theta > \theta_c \\ \left(\frac{\theta-\theta_{wilt}}{\theta_c-\theta_{wilt}}\right) \text{ for } \theta_{wilt} < \theta \leq \theta_c \\ 0 \; for \; \theta < \theta_{wilt} \end{cases}$
Modulate photosynthesis through modifying V_{max} in fall		$e(t) = \frac{1}{1+(t/t_0)^b}$, where t is the Julian day [*Wilson et al.*, 2000]; parameters t_0 and b were obtained from fits to four key dates derived from MODIS phenology observations [*Zhang et al.*, 2003]	
K_c and K_o (mol mol^{-1}), Michaelis-Menten parameters for CO_2 and oxygen, respectively	$K_1 = 1.5\ 10^{-4} \exp\left[6000\left(\frac{1}{288.15} - \frac{1}{T}\right)\right]$ $K_2 = 0.25 \exp\left[-1500\left(\frac{1}{288.15} - \frac{1}{T}\right)\right]$	$K_1 = 1.5\ 10^{-4} \exp\left[6000\left(\frac{1}{288.15} - \frac{1}{T}\right)\right]$ $K_2 = 0.836 \exp\left[-1400\left(\frac{1}{288.15} - \frac{1}{T}\right)\right]$	

efficiency over time is suggested from studies of a few tropical tree species that produce tree rings. For example, *Brienen et al*. [2012] analyzed stable isotope concentrations in tree rings of *Mimosa acontholoba*, a dry forest species in Mexico, and found a 40% increase in water use efficiency over the last four decades.

The spatial variability of the change in biomass and growth rates across the monitoring sites was not well reproduced by the DGVMs, all of which showed generally homogeneous change across the study area. The lack of agreement is a combination of the coarse representation of biophysical properties in the models and the scale mismatch between observations (point based) and the numerical models ($1 \times 1°$ horizontal resolution). For example, plot-level values of biomass change are closely associated with tree mortality between annual censuses. Tree mortality is a highly stochastic process, exhibiting considerable interannual variation, a process the models do not incorporate. Additionally, there is an intrinsic variability of field data even between nearby plots, due to strong local climatic, edaphic, or geographic heterogeneity associated with subgrid scale properties the models cannot include. Soil physical properties (e.g., texture, depth, and bulk density) have been shown to be important predictors of forest dynamics, including mortality rates, in Amazonia [*Quesada et al*., 2012]. The simulations were run using a default soil depth throughout the study area and a gridded soil texture map, which do not capture the fine-scale three-dimensional variation in soil properties. Furthermore, the simplistic nature of plant functional type (PFT) classifications used in the DGVMs in this study ignores regional differences in plant composition and life history strategies across Amazonia. Although the RAINFOR data set represent the most comprehensive data set of rainforest biomass available today, it does not have the characteristics of a large-scale forest inventory. Therefore, we caution that DGVM estimates of forest dynamics are only comparable at large spatial and long time scales. The National Forest Inventory that is being conducted by the Brazilian Forest Service should be concluded in 2017 and will provide more representative data to validate models.

Appendix A

Table A2. The Canopy Physiological Processes Governing Stomatal Conductance and How They Control Water and CO_2 Fluxes in the Vegetation Canopy for Each of the Numerical Models IBIS, ED2, and JULES are Described in Detail

	IBIS [*Foley et al*., 1996; *Kucharik et al*., 2000]	ED2 [*Medvigy et al*., 2009; *Moorcroft et al*., 2001]	JULES [*Best et al*., 2011; *Clark et al*., 2011; *Cox et al*., 1998]
	Semiempirical models based on *Ball et al*. [1986], *Collatz et al*. [1991], *Dewar* [1995], and *Lloyd and Farquhar* [1994]		
Stomatal conductance of water vapor (mol H_2O m^{-2} s^{-1})	$g_{s,H_2O} = \frac{mA_n}{(C_s-\Gamma)\left(1+\frac{D_s}{D_o}\right)} + b$ [*Leuning*, 1995] where m and b are slope and intercept of the conductance-photosynthesis relationship, respectively, C_s is CO_2 concentration (mol mol^{-1}) at leaf surface, D_s is water vapor mole fraction difference between leaf and air (mol mol^{-1}), and C_i is CO_2 concentration (mol mol^{-1}) at the intracellular air spaces of the leaf; First-order diffusion equations $C_i = C_s - \frac{1.6\ A_n}{g_{s,H_2O}}$	(same as IBIS)	$C_i = C_s - \frac{1.6\ A_n}{g_{s,H_2O}}$ where C_s is CO_2 partial pressure (Pa) at leaf surface, C_i partial pressure (Pa) in the intracellular air spaces of the leaf $\frac{C_i-\Gamma}{C_s-\Gamma} = f_0\left(1-\frac{D}{D*}\right)$ [*Jacobs*, 1994], where Γ is the CO_2 compensation point (Pa) and f_0 and $D*$ are PFT-specific calibration parameters
Boundary layer conductance for water vapor (mol H_2O m^{-2} s^{-1})		$g_{b,H_2O} = 10.75\ g_{bh}$ where g_{bh} is the boundary layer conductance defined as a function of wind speed and leaf shape [*Medvigy et al*., 2009] $C_s = C_a - \frac{A_n}{1.4\ \ g_{b,H_2O}}$	
Boundary layer conductance for CO_2 (mol CO_2 m^{-2} s^{-1})	$C_s = C_a - \frac{A_n}{g_{s,CO_2}}$ where C_s is CO_2 concentration (mol mol^{-1}) at leaf surface, C_a is the fraction of CO_2 (mol mol^{-1}) in the atmosphere	$C_S = C_a - \frac{A_n}{g_{s,CO_2}}$	

Acknowledgments
The data for model simulation used in this work is available upon request to the corresponding author (adacastanho@gmail.com). We gratefully thank Gordon and Betty Moore Foundation grant 3413 and 1971 and CNPq (*Bolsa Jovens Talentos*, process 400079/2013-5) for funding this work. We would like to thank the following people for their contributions: Oliver Phillips and Gabriela Lopez Gonzales for valuable discussions about the RAINFOR database, Eric Davidson for valuable discussions, Paul Lefebvre for creative solutions in graphic representations, Naomi Levine and Marcos Longo for preparation of soil texture and climatological data set, and all people involved in this model inter-comparison project. We thank the anonymous referees for the valuable comments on the review of the manuscript.

References

Aragão, L. E. O. C., B. Poulter, J. B. Barlow, L. O. Anderson, Y. Malhi, S. Saatchi, O. L. Phillips, and E. Gloor (2014), Environmental change and the carbon balance of Amazonian forests, *Biol. Rev.*, *89*, 913–931, doi:10.1111/brv.12088.

Baker, T. R., et al. (2004), Increasing biomass in Amazonian forest plots, *Philos. Trans. R. Soc. London Ser. B Biol. Sci.*, *359*(1443), 353–365, doi:10.1098/rstb.2003.1422.

Balch, J. K., et al. (2015), The tolerance and susceptibility of Amazon forest to fire: Insights from large-scale experimental burns, *BioScience*, *65*, 893–905.

Ball, J. T., I. E. Woodrow, and J. A. Berry (1986), A model predicting stomatal conductance and its contribution to the control of photosynthesis under different environmental conditions, in *Photosynthesis' Research*, edited by J. Biggins, pp. 221–224, Martinus Nijhoff, Netherlands.

Best, M. J., et al. (2011), The Joint UK Land Environment Simulator (JULES), model description—Part 1: Energy and water fluxes, *Geosci. Model Dev.*, *4*(3), 677–699, doi:10.5194/gmd-4-677-2011.

Botta, A., N. Ramankutty, and J. A. Foley (2002), Long-term variations of climate and carbon fluxes over the Amazon basin, *Geophys. Res. Lett.*, *29*(9), 1319, doi:10.1029/2001GL013607.

Brando, P. M., D. C. Nepstad, J. K. Balch, B. Bolker, M. C. Christman, M. Coe, and F. E. Putz (2012), Fire-induced tree mortality in a neotropical forest: The roles of bark traits, tree size, wood density and fire behavior, *Global Change Biol.*, *18*(2), 630–641, doi:10.1111/j.1365-2486.2011.02533.x.

Brando, P. M., et al. (2014), Abrupt increases in Amazonian tree mortality due to drought-fire interactions, *Proc. Natl. Acad. Sci. U.S.A.*, *111*(17), 6347–6352, doi:10.1073/pnas.1305499111.

Brienen, R. J. W., E. Gloor, and P. A. Zuidema (2012), Detecting evidence for CO_2 fertilization from tree ring studies: The potential role of sampling biases, *Global Biogeochem. Cycles*, *26*, GB1025, doi:10.1029/2011GB004143.

Castanho, A. D. A., M. T. Coe, M. H. Costa, Y. Malhi, D. Galbraith, and C. A. Quesada (2013), Improving simulated Amazon forest biomass and productivity by including spatial variation in biophysical parameters, *Biogeosciences*, *10*(4), 2255–2272, doi:10.5194/bg-10-2255-2013.

Chave, J., et al. (2005), Tree allometry and improved estimation of carbon stocks and balance in tropical forests, *Oecologia*, *145*(1), 87–99, doi:10.1007/s00442-005-0100-x.

Clark, D. B., D. A. Clark, and S. F. Oberbauer (2010), Annual wood production in a tropical rain forest in NE Costa Rica linked to climatic variation but not to increasing CO_2, *Global Change Biol.*, *16*(2), 747–759, doi:10.1111/j.1365-2486.2009.02004.x.

Clark, D. B., et al. (2011), The Joint UK Land Environment Simulator (JULES), model description—Part 2: Carbon fluxes and vegetation dynamics, *Geosci. Model Dev.*, *4*(3), 701–722, doi:10.5194/gmd-4-701-2011.

Coe, M. T., et al. (2013), Deforestation and climate feedbacks threaten the ecological integrity of south–southeastern Amazonia, *Philos. Trans. R. Soc. B Biol. Sci.*, *368*(1619), doi:10.1098/rstb.2012.0155.

Collatz, G. J., J. T. Ball, C. Grivet, and J. A. Berry (1991), Physiological and environmental regulation of stomatal conductance, photosynthesis and transpiration: A model that includes a laminar boundary layer, *Agric. For. Meteorol.*, *54*(2–4), 107–136, doi:10.1016/0168-1923(91)90002-8.

Collatz, G., M. Ribas-Carbo, and J. Berry (1992), Coupled photosynthesis-stomatal conductance model for Leaves of C_4 Plants, *Funct. Plant Biol.*, *19*(5), 519–538, doi:10.1071/PP9920519.

Costa, M. H., M. T. Coe, and J. L. Guyot (2009), Effects of climatic variability and deforestation on surface water regimes, in *Amazonia and Global Change* edited, pp. 543–553, AGU, Washington, D. C.

Cox, P. M., C. Huntingford, and R. J. Harding (1998), A canopy conductance and photosynthesis model for use in a GCM land surface scheme, *J. Hydrol.*, *212–213*, 79–94, doi:10.1016/S0022-1694(98)00203-0.

Delbart, N., P. Ciais, J. Chave, N. Viovy, Y. Malhi, and T. Le Toan (2010), Mortality as a key driver of the spatial distribution of aboveground biomass in Amazonian forest: Results from a dynamic vegetation model, *Biogeosciences*, *7*(10), 3027–3039, doi:10.5194/bg-7-3027-2010.

Dewar, R. C. (1995), Interpretation of an empirical model for stomatal conductance in terms of guard cell function, *Plant Cell Environ.*, *18*(4), 365–372, doi:10.1111/j.1365-3040.1995.tb00372.x.

Espirito-Santo, F. D., et al. (2014), Size and frequency of natural forest disturbances and the Amazon forest carbon balance, *Nat. Commun.*, *5*, 3434, doi:10.1038/ncomms4434.

Eva, H. D., et al. (2005), A proposal for defining the geographical boundaries of Amazonia Report, Eurpean Communities, Luxembourg.

Farquhar, G. D., S. von Caemmerer, and J. A. Berry (1980), A biochemical model of photosynthetic CO2 assimilation in leaves of C3 species, *Planta*, *149*(1), 78–90, doi:10.1007/BF00386231.

Foley, J. A., I. C. Prentice, N. Ramankutty, S. Levis, D. Pollard, S. Sitch, and A. Haxeltine (1996), An integrated biosphere model of land surface processes, terrestrial carbon balance, and vegetation dynamics, *Global Biogeochem. Cycles*, *10*(4), 603–628, doi:10.1029/96GB02692.

Foley, J. A., et al. (2011), Solutions for a cultivated planet, *Nature*, *478*(7369), 337–342. [Available at http://www.nature.com/nature/journal/v478/n7369/abs/nature10452.html#supplementary-information.]

Galbraith, D., P. E. Levy, S. Sitch, C. Huntingford, P. Cox, M. Williams, and P. Meir (2010), Multiple mechanisms of Amazonian forest biomass losses in three dynamic global vegetation models under climate change, *New Phytol.*, *187*(3), 647–665, doi:10.1111/j.1469-8137.2010.03350.x.

Galbraith, D., et al. (2013), Residence times of woody biomass in tropical forests, *Plant Ecol. Diversity*, *6*(1), 139–157, doi:10.1080/17550874.2013.770578.

Gatti, L. V., et al. (2014), Drought sensitivity of Amazonian carbon balance revealed by atmospheric measurements, *Nature*, *506*(7486), 76–80, doi:10.1038/nature12957.

Green, W. H., and G. A. Ampt (1911), Studies on soil physics: 1. The flow of air and water through soils, *J. Agric. Sci.*, *4*, 1–24.

Houghton, R. (2014), Land management options for mitigation and adaptation to climate change, in *Global Environmental Change*, edited by B. Freedman, pp. 389–398, Springer, Netherlands.

Huntingford, C., et al. (2013), Simulated resilience of tropical rainforests to CO_2-induced climate change, *Nat. Geosci.*, *6*(4), 268–273, doi:10.1038/ngeo1741.

Hurtt, G. C., S. Frolking, M. G. Fearon, B. Moore, E. Shevliakova, S. Malyshev, S. W. Pacala, and R. A. Houghton (2006), The underpinnings of land-use history: Three centuries of global gridded land-use transitions, wood-harvest activity, and resulting secondary lands, *Global Change Biol.*, *12*(7), 1208–1229, doi:10.1111/j.1365-2486.2006.01150.x.

Jacobs, C. M. J. (1994), Direct impact of atmopsheric CO_2 enrichment on regional transpiration.

Kucharik, C. J., J. A. Foley, C. Delire, V. A. Fisher, M. T. Coe, J. D. Lenters, C. Young-Molling, N. Ramankutty, J. M. Norman, and S. T. Gower (2000), Testing the performance of a dynamic global ecosystem model: Water balance, carbon balance, and vegetation structure, *Global Biogeochem. Cycles*, *14*(3), 795–825, doi:10.1029/1999GB001138.

Le Quere, C., et al. (2009), Trends in the sources and sinks of carbon dioxide, *Nat. Geosci.*, *2*(12), 831–836. [Available at http://www.nature.com/ngeo/journal/v2/n12/suppinfo/ngeo689_S1.html.]

Leuning, R. (1995), A critical appraisal of a combined stomatal-photosynthesis model for C3 plants, *Plant Cell Environ.*, *18*(4), 339–355, doi:10.1111/j.1365-3040.1995.tb00370.x.

Lewis, L. S., et al. (2004a), Tropical forest tree mortality, recruitment and turnover rates: Calculation, interpretation and comparison when census intervals vary, *J. Ecol.*, *92*(6), 929–944, doi:10.2307/3599736.

Lewis, S. L., Y. Malhi, and O. L. Phillips (2004b), Fingerprinting the impacts of global change on tropical forests, *Philos. Trans. R. Soc. London Ser. B Biol. Sci.*, *359*(1443), 437–462, doi:10.1098/rstb.2003.1432.

Lewis, S. L., et al. (2004c), Concerted changes in tropical forest structure and dynamics: Evidence from 50 South American long-term plots, *Philos. Trans. R. Soc. London Ser. B Biol. Sci.*, *359*(1443), 421–436, doi:10.1098/rstb.2003.1431.

Lewis, S. L., J. Lloyd, S. Sitch, E. T. A. Mitchard, and W. F. Laurance (2009), Changing ecology of tropical forests: Evidence and drivers, *Annu. Rev. Ecol. Evol. Syst.*, *40*(1), 529–549, doi:10.1146/annurev.ecolsys.39.110707.173345.

Li, K. Y., M. T. Coe, and N. Ramankutty (2005), Investigation of hydrological variability in West Africa using land surface models, *J. Clim.*, *18*(16), 3173–3188.

Lloyd, J., and G. D. Farquhar (1994), 13C discrimination during CO_2 assimilation by the terrestrial biosphere, *Oecologia*, *99*(3/4), 201–215, doi:10.2307/4220751.

Lloyd, J., and G. D. Farquhar (1996), The CO2 dependence of photosynthesis, plant growth responses to elevated atmospheric CO_2 concentrations and their interaction with soil nutrient status, *Funct. Ecol.*, *10*(1), 4–32.

Malhi, Y. (2010), The carbon balance of tropical forest regions, 1990–2005, *Curr. Opin. Environ. Sustainability*, *2*(4), 237–244, doi:10.1016/j.cosust.2010.08.002.

Malhi, Y., and J. Wright (2004), Spatial patterns and recent trends in the climate of tropical rainforest regions, *Philos. Trans. R. Soc. London Ser. B Biol. Sci.*, *359*(1443), 311–329, doi:10.1098/rstb.2003.1433.

Malhi, Y., et al. (2002), An international network to monitor the structure, composition and dynamics of Amazonian forests (RAINFOR), *J. Veg. Sci.*, *13*(3), 439–450, doi:10.1111/j.1654-1103.2002.tb02068.x.

Malhi, Y., et al. (2004), The above-ground coarse wood productivity of 104 neotropical forest plots, *Global Change Biol.*, *10*(5), 563–591, doi:10.1111/j.1529-8817.2003.00778.x.

Malhi, Y., et al. (2006), The regional variation of aboveground live biomass in old-growth Amazonian forests, *Global Change Biol.*, *12*(7), 1107–1138, doi:10.1111/j.1365-2486.2006.01120.x.

Malhi, Y., L. E. Aragao, D. Galbraith, C. Huntingford, R. Fisher, P. Zelazowski, S. Sitch, C. McSweeney, and P. Meir (2009), Exploring the likelihood and mechanism of a climate-change-induced dieback of the Amazon rainforest, *Proc. Natl. Acad. Sci. U.S.A.*, *106*(49), 20,610–20,615, doi:10.1073/pnas.0804619106.

Malhi, Y., C. Doughty, and D. Galbraith (2011), The allocation of ecosystem net primary productivity in tropical forests, *Philos. Trans. R. Soc. London Ser. B Biol. Sci.*, *366*(1582), 3225–3245, doi:10.1098/rstb.2011.0062.

Marengo, J. A., C. A. Nobre, J. Tomasella, M. F. Cardoso, and M. D. Oyama (2008), Hydro-climatic and ecological behaviour of the drought of Amazonia in 2005, *Philos. Trans. R. Soc. B Biol. Sci.*, *363*(1498), 1773–1778, doi:10.1098/rstb.2007.0015.

Medvigy, D., S. C. Wofsy, J. W. Munger, D. Y. Hollinger, and P. R. Moorcroft (2009), Mechanistic scaling of ecosystem function and dynamics in space and time: Ecosystem Demography model version 2, *J. Geophys. Res.*, *114* G01002, doi:10.1029/2008JG000812.

Moorcroft, P. R., G. C. Hurtt, and S. W. Pacala (2001), A method for scaling vegetation dynamics: The Ecosystem Demography model (Ed), *Ecol. Monogr.*, *71*(4), 557–586, doi:10.1890/0012-9615(2001)071[0557:AMFSVD]2.0.CO;2.

Muller-Landau, H. C. (2009), Sink in the African Jungle, *Nature*, *457*, 969–970.

Pan, Y., et al. (2011), A large and persistent carbon sink in the world's forests, *Science*, *333*(6045), 988–993, doi:10.1126/science.1201609.

Peacock, J., T. R. Baker, S. L. Lewis, G. Lopez-Gonzalez, and O. L. Phillips (2007), The RAINFOR database: Monitoring forest biomass and dynamics, *J. Veg. Sci.*, *18*(4), 535–542, doi:10.1111/j.1654-1103.2007.tb02568.x.

Phillips, O. L., et al. (1998), Changes in the carbon balance of tropical forests: Evidence from long-term plots, *Science*, *282*(5388), 439–442, doi:10.1126/science.282.5388.439.

Phillips, O. L., et al. (2002), Increasing dominance of large lianas in Amazonian forests, *Nature*, *418*(6899), 770–774. [Available at http://www.nature.com/nature/journal/v418/n6899/suppinfo/nature00926_S1.html.]

Phillips, O. L., S. L. Lewis, T. R. Baker, K.-J. Chao, and N. Higuchi (2008), The changing Amazon forest, *Philos. Trans. R. Soc. B Biol. Sci.*, *363*(1498), 1819–1827, doi:10.1098/rstb.2007.0033.

Phillips, O. L., et al. (2009), Drought sensitivity of the Amazon rainforest, *Science*, *323*(5919), 1344–1347, doi:10.1126/science.1164033.

Poulter, B., F. Hattermann, E. D. Hawkins, S. Zaehle, S. Sitch, N. Restrepo-Coupe, U. Heyder, and W. Cramer (2010), Robust dynamics of Amazon dieback to climate change with perturbed ecosystem model parameters, *Global Change Biol.*, *16*(9), 2476–2495, doi:10.1111/j.1365-2486.2009.02157.x.

Powell, T. L., et al. (2013), Confronting model predictions of carbon fluxes with measurements of Amazon forests subjected to experimental drought, *New Phytol.*, *200*(2), 350–365, doi:10.1111/nph.12390.

Quesada, C. A., et al. (2012), Basin-wide variations in Amazon forest structure and function are mediated by both soils and climate, *Biogeosciences*, *9*(6), 2203–2246, doi:10.5194/bg-9-2203-2012.

Rammig, A., T. Jupp, K. Thonicke, B. Tietjen, J. Heinke, S. Ostberg, W. Lucht, W. Cramer, and P. Cox (2010), Estimating the risk of Amazonian forest dieback, *New Phytol.*, *187*(3), 694–706, doi:10.1111/j.1469-8137.2010.03318.x.

Reichstein, M., et al. (2013), Climate extremes and the carbon cycle, *Nature*, *500*(7462), 287–295, doi:10.1038/nature12350.

Sakaguchi, K., X. Zeng, B. J. Christoffersen, N. Restrepo-Coupe, S. R. Saleska, and P. M. Brando (2011), Natural and drought scenarios in an east central Amazon forest: Fidelity of the Community Land Model 3.5 with three biogeochemical models, *J. Geophys. Res.*, *116* G01029, doi:10.1029/2010JG001477.

Sheffield, J., G. Goteti, and E. F. Wood (2006), Development of a 50-Year High-Resolution Global Dataset of Meteorological Forcings for Land Surface Modeling, *J. Clim.*, *19*, 3088–3111, doi:10.1175/JCLI3790.1.

van der Heijden, G. M., S. A. Schnitzer, J. S. Powers, and O. L. Phillips (2013), Liana impacts on carbon cycling, storage and sequestration in tropical forests, *Biotropica*, *45*(6), 682–692, doi:10.1111/btp.12060.

Wilson, K. B., D. D. Baldocchi, and P. J. Hanson (2000), Quantifying stomatal and non-stomatal limitations to carbon assimilation resulting from leaf aging and drought in mature deciduous tree species, *Tree Physiol.*, *20*, 787–797.

Wright, S. J. (2005), Tropical forests in a changing environment, *Trends Ecol. Evol.*, *20*(10), 553–560, doi:10.1016/j.tree.2005.07.009.

Wright, S. J. (2013), The carbon sink in intact tropical forests, *Global Change Biol.*, *19*(2), 337–339, doi:10.1111/gcb.12052.

Zhang, K., et al. (2015), The fate of Amazonian ecosystems over the coming century arising from changes in climate, atmospheric CO_2, and land use, *Global Change Biol.*, *21*(7), 2569–2587, doi:10.1111/gcb.12903.

Zhang, X., M. A. Friedl, C. B. Schaaf, A. H. Strahler, J. C. F. Hodges, F. Gao, B. C. Reed, and A. Huete (2003), Monitoring vegetation phenology using MODIS, *Remote Sens. Environ.*, *84*(3), 471–475, doi:10.1016/S0034-4257(02)00135-9.

Zscheischler, J., M. Reichstein, S. Harmeling, A. Rammig, E. Tomelleri, and M. D. Mahecha (2014), Extreme events in gross primary production: A characterization across continents, *Biogeosciences*, *11*(11), 2909–2924, doi:10.5194/bg-11-2909-2014.